iScience

CellPress
OPEN ACCESS

Article

NANOS2 suppresses the cell cycle by repressing mTORC1 activators in embryonic male germ cells

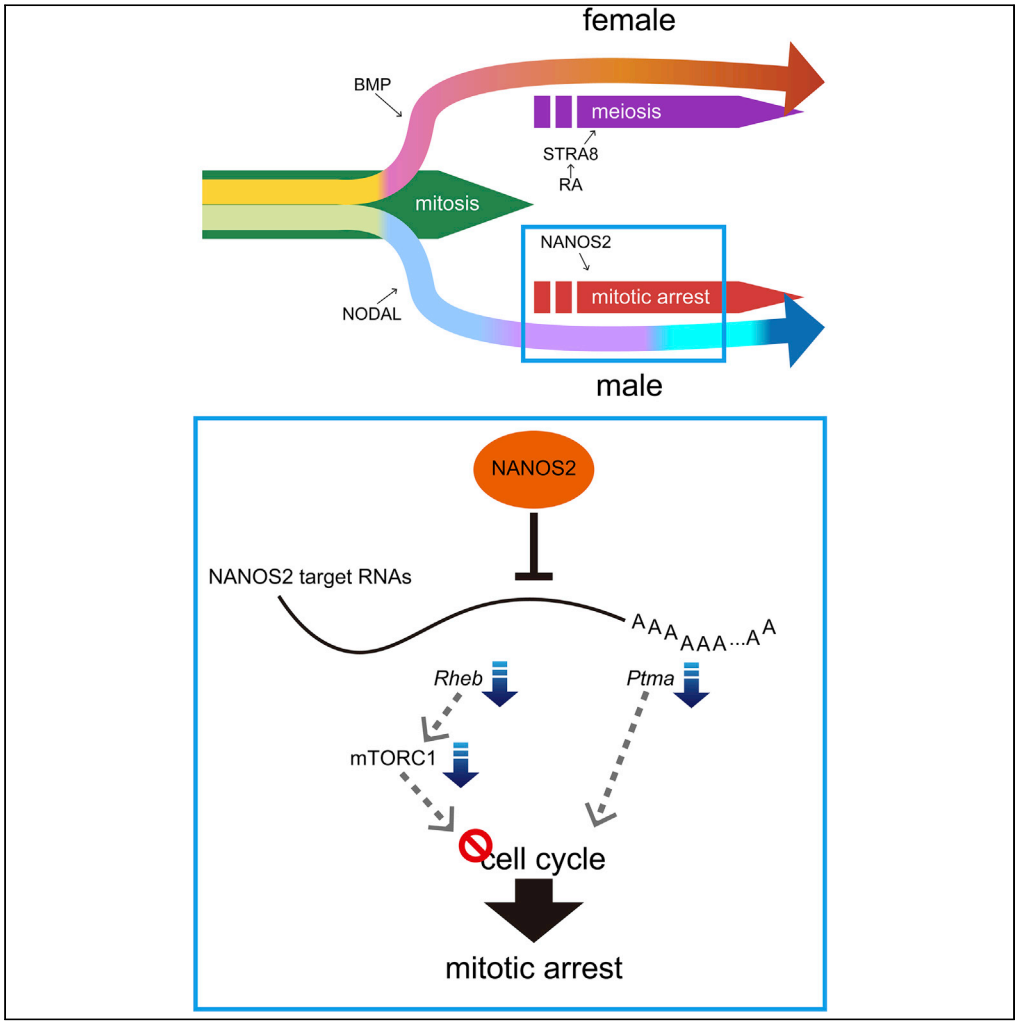

Ryuki Shimada, Hiroko Koike, Takamasa Hirano, Yuzuru Kato, Yumiko Saga

ysaga@nig.ac.jp

Highlights

Single-cell RNA-seq data recapitulated sexual differentiation processes

Cell cycle state of developing germ cells was revealed by single-cell RNA-seq data

NANOS2 suppresses mTORC1 activators to induce cell cycle arrest of germ cells

Shimada et al., iScience 24, 102890
August 20, 2021
https://doi.org/10.1016/j.isci.2021.102890

iScience

CellPress
OPEN ACCESS

Article

NANOS2 suppresses the cell cycle by repressing mTORC1 activators in embryonic male germ cells

Ryuki Shimada,[1,2,5] Hiroko Koike,[1,6] Takamasa Hirano,[2] Yuzuru Kato,[1,2] and Yumiko Saga[1,2,3,4,7,*]

SUMMARY

During murine germ cell development, male germ cells enter the mitotically arrested G0 stage, which is an initial step of sexually dimorphic differentiation. The male-specific RNA-binding protein NANOS2 has a key role in suppressing the cell cycle in germ cells. However, the detailed mechanism of how NANOS2 regulates the cell cycle remains unclear. Using single-cell RNA sequencing (scRNA-seq), we extracted the cell cycle state of each germ cell in wild-type and *Nanos2*-KO testes and revealed that *Nanos2* expression starts in mitotic cells and induces mitotic arrest. We identified *Rheb*, a regulator of mTORC1, and *Ptma* as possible targets of NANOS2. We propose that repression of the cell cycle is a primary function of NANOS2 and that it is mediated via the suppression of mTORC1 activity through the repression of *Rheb* in a post-transcriptional manner.

INTRODUCTION

The sexually differentiated gametes sperm and eggs originally differentiate from common precursors, primordial germ cells (PGCs). PGCs are specified at the posterior end of gastrulating embryos at E7.25 and migrate toward the gonads in mice (Hayashi et al., 2007; Anderson et al., 2000). After colonizing the gonads, PGCs start sex-specific differentiation by responding to factors supplied from surrounding somatic cells. In ovaries, retinoic acid (RA) from the mesonephros induces the expression of meiosis initiators, *Stimulated by RA gene 8* (*Stra8*) and *Meiosis initiator* (*Meiosin*), in germ cells to start meiosis (Koubova et al., 2006; Anderson et al., 2008; Ishiguro et al., 2020). On the other hand, in testes, RA is degraded by CYP26B1 produced in somatic cells (Saba et al., 2014b; Bowles et al., 2006), thus germ cells cannot enter meiosis. Instead, male germ cells enter mitotic arrest from E13.5 and most are arrested at the G1/G0 phase at E15.5 (Western et al., 2008). Therefore, sexual differentiation of PGCs is closely associated with distinct cell cycle regulation.

Although the initiation mechanism of mitotic arrest in male germ cells remains unclear, several factors have been identified as regulators of the cell cycle. Retinoblastoma 1 (RB1), a major cell cycle regulator involved in cell proliferation, apoptosis and cell differentiation in somatic cells (Zacksenhaus et al., 1996), and p38 mitogen-activated protein kinase (MAPK), which is activated by several types of cellular stress (Ono and Han 2000), were previously suggested as regulators of mitotic arrest in male germ cells (Spiller et al., 2010; Ewen et al., 2010). However, the relationships among these cascades are unclear.

An evolutionarily conserved RNA-binding protein, NANOS2, was previously identified as an essential factor for male germ cell differentiation (Tsuda et al., 2003). NANOS2 protein is expressed in the testes from E13.5 and promotes male-type gene expression such as DNMT3L and TDRD9 (Suzuki and Saga 2008; Suzuki et al., 2016). NANOS2 is also involved in cell cycle regulation. In the absence of NANOS2, male germ cells are arrested at G0 at E14.5 but resume the cell cycle at E15.5 (Suzuki and Saga 2008; Saba et al., 2014a). Therefore, NANOS2 was suggested to function in maintaining the arrested cell cycle.

NANOS2 interacts with another RNA-binding protein, DND1, and a deadenylation component, CNOT1, and localizes to processing bodies, by which the expression of recruited RNAs may be repressed (Suzuki et al, 2010, 2012, 2016; Parker and Sheth 2007; Decker and Parker 2012; Shimada et al., 2019). In this cascade, DND1 is involved in the target recognition together with NANOS2. We also reported that the

[1]Department of Genetics, SOKENDAI, Yata 1111, Mishima, Shizuoka 411-8540, Japan

[2]Mammalian Development Laboratory, Department of Gene Function and Phenomics, National Institute of Genetics, Yata 1111, Mishima, Shizuoka 411-8540, Japan

[3]Division for the Development of Genetically Engineered Mouse Resources, Genetic Resource Center, National Institute of Genetics, Yata 1111, Mishima, Shizuoka 411-8540, Japan

[4]Department of Biological Sciences, Graduate School of Science, The University of Tokyo, Tokyo 113-0033, Japan

[5]Present address: Department of Chromosome Biology, Institute of Molecular Embryology and Genetics (IMEG), Kumamoto University, Kumamoto 860-0811, Japan

[6]Present address: Quality Assurance, Johnson & Johnson K.K. Medical Company, 5-2, Nishikanda 3-chome, Chiyoda-ku, Tokyo 101-0065, Japan

[7]Lead contact

*Correspondence: ysaga@nig.ac.jp

https://doi.org/10.1016/j.isci.2021.102890

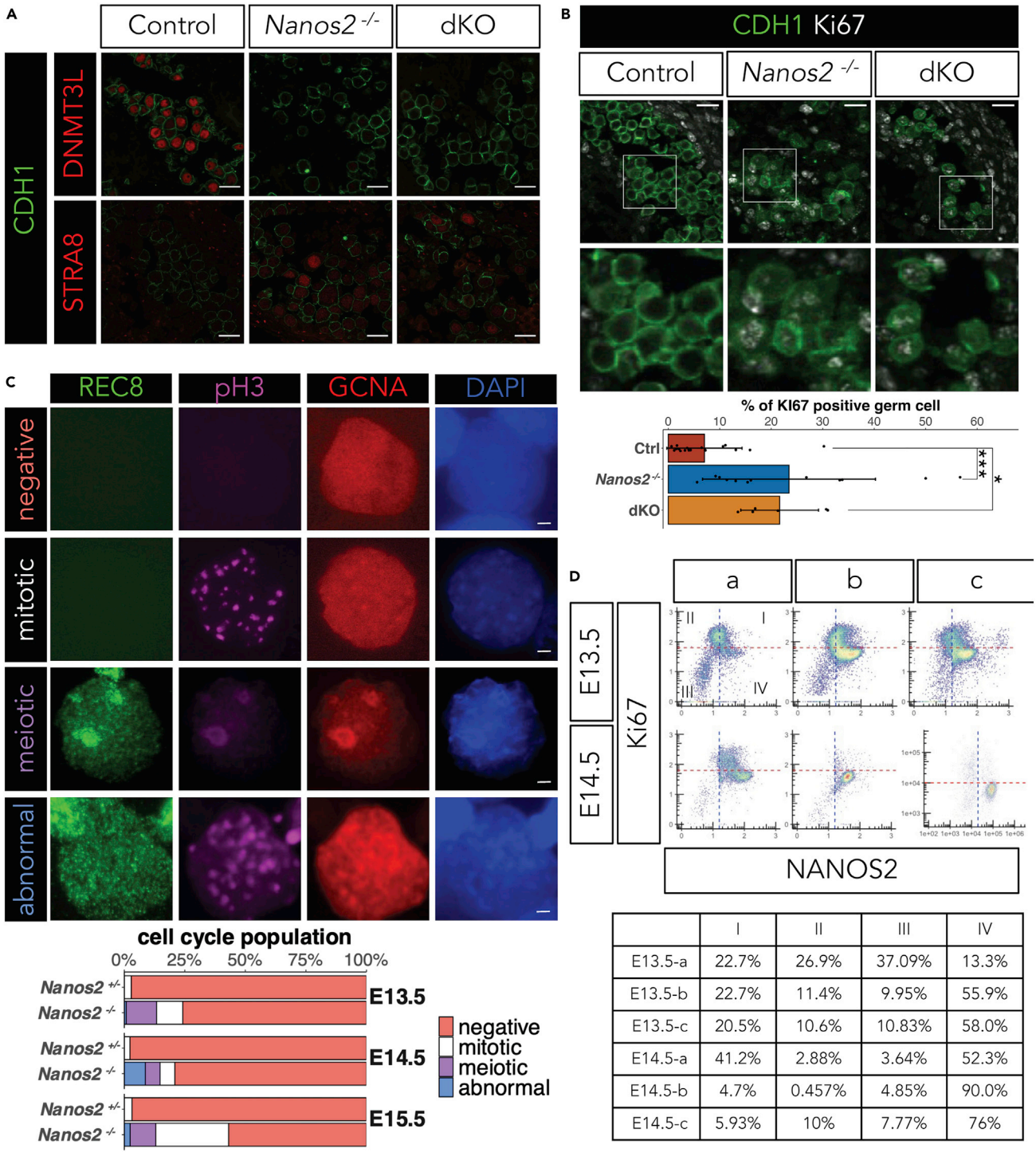

	I	II	III	IV
E13.5-a	22.7%	26.9%	37.09%	13.3%
E13.5-b	22.7%	11.4%	9.95%	55.9%
E13.5-c	20.5%	10.6%	10.83%	58.0%
E14.5-a	41.2%	2.88%	3.64%	52.3%
E14.5-b	4.7%	0.457%	4.85%	90.0%
E14.5-c	5.93%	10%	7.77%	76%

Figure 1. NANOS2 has functions separate from the suppression of *Dazl*

(A and B) Immunofluorescence analyses of testes from control, *Nanos2* $^{-/-}$ and *Dazl*; *Nanos2*-dKO at E15.5. Tamoxifen was injected at E12.5. Control includes both *Nanos2* $^{+/+}$ and *Nanos2* $^{+/-}$. Markers used for (A) are the male differentiation marker, DNMT3L (red, upper), meiosis marker, STRA8 (red, lower), and germ cell marker, CDH1 (green). Markers used for (B) are the mitosis marker, Ki67 (white) and germ cell marker, CDH1 (green). Magnified images in squares are also shown in (B). The quantified data shown below are represented as mean with SD (B). ***$p < 0.001$ and *$p < 0.05$ (Dunnett's test). Scale bars: 20 μm.

(C) Classification of male germ cells by immunofluorescence analysis with meiosis, REC8 (green), mitosis, pH3 (magenta), and germ cell, GCNA (red) markers. Representative images were collected from E15.5 samples of *Nanos2* $^{+/-}$ and *Nanos2* $^{-/-}$. Quantification of *Nanos2* $^{+/-}$ and *Nanos2* $^{-/-}$ germ cells based on

Figure 1. *Continued*

the classification at E13.5, E14.5 and E15.5. The bar graph is composed of negative ($REC8^-/pH3^-$: including mitotic arrest, orange), mitotic ($REC8^-/pH3^+$, white), meiotic ($REC8^+/pH3^-$, purple), and abnormal ($REC8^+/pH3^+$, blue). Scale bars: 1 μm.

(D) Flow cytometric analysis of germ cells obtained from wild-type testes at E13.5 and E14.5. Cells were stained with anti-NANOS2 and anti-Ki67 antibodies. The blue dashed lines indicate the threshold of NANOS2 signal (see also Figures S2 and S3). The red dashed lines indicate the threshold of Ki67 signal. According to NANOS2 signal intensities, plots were aligned from left to right to reflect germ cell development. Each plot indicates a biological sample. Three biological replicates are shown for both E13.5 and E14.5. The table below the plots indicates the percentage of cells plotted on each I-IV region.

association between NANOS2 and DND1 is important to maintain DND1 protein stability because the DND1 protein level decreases in the absence of NANOS2 even though its mRNA is unaffected (Wright et al., 2021). Possible target RNAs regulated by NANOS2 have been searched by several strategies, including NANOS2-IP to detect interacting RNAs, and expression change analyses using *Nanos2*-KO and *Nanos2*-overexpression. However, only two genes have been identified as bona fide NANOS2 targets (Kato et al., 2016; Zhou et al., 2015). One is *Dazl*, which is strongly expressed in germ cells just after colonizing the gonads in both males and females (Seligman and Page 1998). DAZL was reported to act as a licensing factor for germ cells to initiate sexual differentiation (Gill et al., 2011). It is required for germ cells to acquire competence to respond to RA to enter meiotic prophase in ovaries, whereas its expression is repressed by NANOS2 once germ cells enter the testes. As mitotic activity is resumed and STRA8 is upregulated in the absence of NANOS2, $Nanos2^{-/-}$ germ cells were thought to be feminized (Suzuki and Saga 2008). However, it is unclear whether the repression of DAZL by NANOS2 is responsible for the maintenance of mitotic arrest and repression of feminization.

To address the above question, we first conducted double KO of NANOS2 and DAZL, and found that DAZL is not the sole factor responsible for cell cycle repression. To explore more factors responsible for cell cycle regulation, we conducted single-cell RNA sequencing (scRNA-seq) analyses and revealed that NANOS2 functions not only to maintain the arrested cell cycle but also to induce mitotic arrest.

RESULTS

Dazl suppression by NANOS2 is not sufficient to repress mitotic resumption

In the previous study, we demonstrated that DAZL expression is suppressed by NANOS2 in a *Dazl* 3′UTR-dependent manner (Kato et al., 2016). The forced expression of DAZL by deleting its 3′-UTR led to the failure of male-type gene expression, meiosis initiation and resumption of mitosis, similar phenotypes of $Nanos2^{-/-}$ germ cells even in the presence of NANOS2 (Kato et al., 2016). Therefore, *Dazl* suppression by NANOS2 is hypothesized to regulate cell differentiation and the cell cycle in male germ cells. To address this issue, we generated *Nanos2* and *Dazl* double knockout (dKO) germ cells only after E12.5 by injecting tamoxifen at E12.5 (see STAR Methods). If *Dazl* suppression by NANOS2 is the main driver of male-type gene expression and cell cycle arrest, the dKO should rescue the phenotype. We stained DNMT3L as a marker of male differentiation, STRA8 as a marker of meiosis initiation and Ki67 as a marker of active mitosis. Contrary to our expectation, DNMT3L expression was not detected and STRA8 was still positive in dKO germ cells (Figure 1A), suggesting that the suppression of *Dazl* by NANOS2 is not sufficient to promote male germ cell differentiation. Importantly, a previous report demonstrated that excess DAZL expression increased the responsiveness of germ cells to RA (Kato et al., 2016). However, the dKO cells exhibited STRA8 expression, suggesting that DAZL is dispensable for germ cells to respond to RA at this point. In addition, dKO cells exhibited positive signals for Ki67 (Figure 1B). After quantification, the proportion of mitotically active cells in the dKO was similar to that in $Nanos2^{-/-}$ testes (Figure 1B). This suggests that there are gene targets of NANOS2 other than *Dazl*.

NANOS2 is required for the initiation of cell cycle arrest

To investigate the mechanism of cell cycle regulation by NANOS2, we re-examined cell cycle states during male germ cell development in $Nanos2^{+/-}$ and $Nanos2^{-/-}$ testes from E13.5 to E15.5. The progression of mitosis and meiosis was examined in each single germ cell by spreading germ cells and co-staining with anti-phosphorylated histone H3 (pH3), a marker of mitotic cells, and anti-REC8, a marker of meiosis, antibodies. In $Nanos2^{+/-}$ testis, we observed two types of cells exhibiting (1) negative signals for both REC8 and pH3, and (2) punctate signals only for pH3 (Figure 1C). The former type likely includes mitotically arrested cells (negative in Figure 1C), whereas the latter type is mitotic cells (mitotic in Figure 1C); the antibody we used exhibits punctate signals in the G2 phase (Hayashi-Takanaka et al., 2009). The majority of cells were classified as negative at E13.5 (97.1%), E14.5 (97.7%), and E15.5

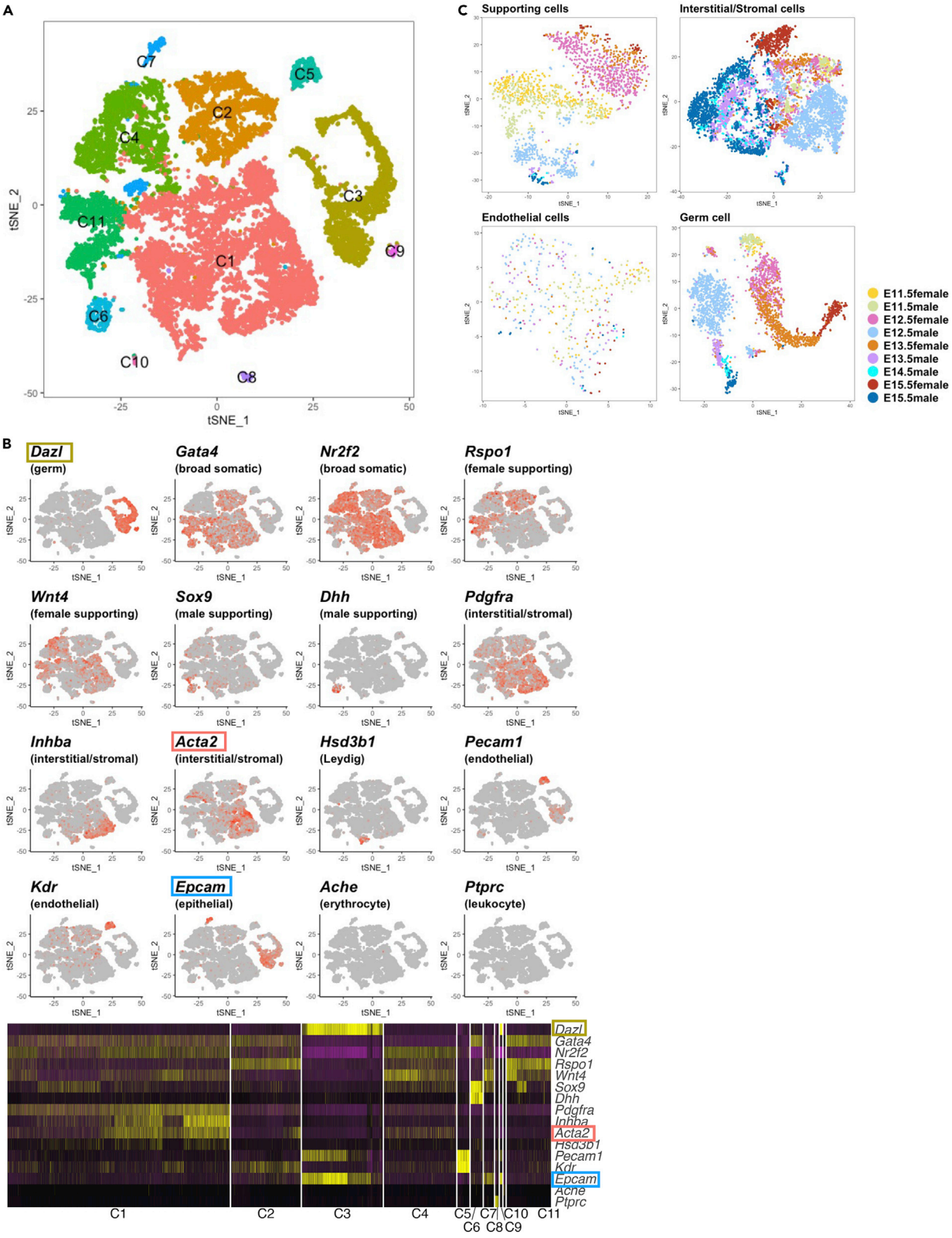
A
C7
C5
C2
C4
C3
C11
C1
C9
C6
C10
C8
tSNE_1
tSNE_2
C
Supporting cells
Interstitial/Stromal cells
Endothelial cells
Germ cell
E11.5female
E11.5male
E12.5female
E12.5male
E13.5female
E13.5male
E14.5male
E15.5female
E15.5male
B
Dazl
(germ)
Gata4
(broad somatic)
Nr2f2
(broad somatic)
Rspo1
(female supporting)
Wnt4
(female supporting)
Sox9
(male supporting)
Dhh
(male supporting)
Pdgfra
(interstitial/stromal)
Inhba
(interstitial/stromal)
Acta2
(interstitial/stromal)
Hsd3b1
(Leydig)
Pecam1
(endothelial)
Kdr
(endothelial)
Epcam
(epithelial)
Ache
(erythrocyte)
Ptprc
(leukocyte)
Dazl
Gata4
Nr2f2
Rspo1
Wnt4
Sox9
Dhh
Pdgfra
Inhba
Acta2
Hsd3b1
Pecam1
Kdr
Epcam
Ache
Ptprc
C1
C2
C3
C4
C5/ C7/ C10 C11
C6 C8 C9

Figure 2. Cell type identification in scRNA-seq data

(A) A tSNE plot for all cells. Each dot indicates a single cell. Cells are colored for each cluster.

(B) Relative expression of selected marker genes is shown. Gene names are written in *italic* and cell types are indicated in parentheses. Cells with high expression are colored darker red (upper panel). The heatmap also shows the relative expression of each gene in each cell. Yellow indicates strong expression and purple indicates weak expression. Cluster numbers are indicated below the plot (lower panel). The gene names surrounded by rectangles are shown in the heatmap in Figure S5.

(C) tSNE plots for supporting, interstitial/stromal, endothelial or germ cells. Cells are colored by embryonic stage.

(97.6%) (Figure 1C), suggesting that mitotic arrest was initiated by E13.5, as previously reported (Western et al., 2008).

We next examined NANOS2$^{-/-}$ germ cells. In addition to negative and mitotic cells, NANOS2$^{-/-}$ germ cells consisted of (3) REC8-single-positive cells and (4) REC8 and pH3-double-positive cells (Figure 1C). The former type is most likely meiotic cells (meiotic in Figure 1C), whereas the latter type was never observed among normal male and female germ cells (Figures 1C and S1). It may be abnormal or dying cells (abnormal in Figure 1C). Based on quantification analysis, the difference between NANOS2$^{+/-}$ and NANOS2$^{-/-}$ germ cells was already evident at E13.5; 24.2% of cells were classified as meiotic or mitotic, although 75.8% of NANOS2$^{-/-}$ germ cells were REC8/pH3-double-negative (negative) (Figure 1C). This raised the possibility that NANOS2 functions not only in the maintenance of mitotic arrest but also in its initiation. Importantly, the proportion of REC8/pH3-double-negative cells did not greatly increase at E14.5 (79.1%). However, it decreased to 56.5% at E15.5 and that of mitotic cells increased (Figure 1C), which is accompanied by the reduction of abnormal cells probably due to the apoptotic cell death.

Although the spreading method is useful to examine the characteristics of each single cell, it may not be accurate to classify cell cycle populations due to the loss of cells and spreading of nuclear components during M phase. To further examine cell cycle states more precisely, we stained germ cells with antibodies against NANOS2, GCNA, and Ki67, and analyzed their signal intensities by fluorescence-activated cell sorting (FACS) at E13.5 and E14.5. Owing to the variation in developmental timing, the results varied at these stages among samples: approximately 20% of cells were identified as germ cells based on the expression of germ cell markers GCNA and NANOS2 in the testes, and the number of NANOS2-positive cells gradually increased with development (Figures S2 and S3). Of note, NANOS2 was detected in the Ki67-positive mitotic cells, suggesting that NANOS2 expression begins prior to the downregulation of Ki67 (Figure 1D). Once NANOS2 was expressed, Ki67 was strongly reduced, supporting the idea that NANOS2 is involved in the initiation of cell cycle arrest.

Characterization of gonadal cell types and their sexual properties based on scRNA-seq data

During embryonic germ cell development, the cell cycle status dynamically changes (Western et al., 2008; Miles et al., 2010). Upon sexual differentiation in particular, marked changes must be induced asynchronously in the transition period from E12.5 to E14.5. To analyze gene expression changes in this transition period and identify the initiation mechanism of mitotic cell cycle arrest, we analyzed the cell cycle state and gene expression profile at single-cell resolution.

We constructed scRNA-seq libraries using E11.5 to E15.5 testes and ovaries and conducted transcriptome analyses. As an excess cell number reduces the sequence depth per cell, we did not conduct deep sequencing for E14.5 female library (see STAR Methods for detail). We summarized the basic information in Figure S4, which includes cell numbers analyzed and read numbers. As we used whole gonads as materials, our data contained information for numerous cell types. The t-SNE plot analysis separated the cells into at least 10 distinct clusters (C1 to C10 in Figure 2A). To identify the cell types of each cluster, we examined representative gene expression in each cluster (Figure S5). Several representative specific cell type markers, such as *Acta2* in C1, *Dppa5a*, *Dppa3* and *Dazl* in C3, *Aldh1a1* in C6, *Epcam* in C7, *C1q* genes in C8, *Rhox* genes in both C3 and C9, *hemoglobin* genes in C10 and *Fst* in C11, were listed. In addition, many genes exhibiting certain cell population-specific expression were observed, demonstrating our scRNA-seq data to be useful to analyze the cell population in developing gonads. Using known distinct genes as markers, we identified the germ cell population and other somatic cell populations (Figure 2B). Importantly, we were able to observe the heterogeneity of gene expression within each cluster, especially in C1, suggesting that more careful analysis can separate more detailed cell types. To evaluate whether our data can be useful to analyze detailed differentiation pathways, such as sexual differentiation, we extracted 4 major cell types in the gonad: germ, supporting, interstitial/stromal, and endothelial cell populations,

and performed clustering analysis for each separately (Figure 2C). Based on the tSNE plot, some of the E11.5 male supporting cells were already separated from female cells and located closer to E12.5 male cells (Figure 2C), indicating that male-type differentiation already started via SRY. Unfortunately, *Sry* itself was not called in our scRNA-seq data. Recently, however, it was reported that *Sry* has an additional exon downstream of the classical exon (Miyawaki et al., 2020). Indeed, our scRNA-seq detected many reads from exon 2 (Figure S6A). In addition to this *Sry* isoform, the downstream genes of SRY, *Sox9* and *Fgf9*, were activated in these cells (Figure S6B). As a counterpart of *Fgf9*, female supporting cells are known to express *Wnt4* to make an ovary (Kim et al., 2006; Jameson et al., 2012). In addition, *Bmp2* was identified as an essential factor to induce female germ cell development and is expressed in female supporting cells (Miyauchi et al., 2017; Wu et al., 2016; Yao et al., 2004; Jameson et al., 2012). We confirmed that *Wnt4* and *Bmp2* expression increased in female supporting cells (Figure S6C). The interstitial/stromal cell population at later stages (E14.5 and E15.5) was clustered based on sex, but these cells were still clustered in a similar position at E12.5, suggesting that their sexual features were determined after the sexual differentiation of supporting cells. The endothelial cells did not exhibit clear segregation based on sex, suggesting that they do not have a clear sexual difference within this time window. At E11.5, germ cells from testes (male, light green) and ovaries (female, light yellow) had almost identical properties, but after E12.5, they exhibited a clear sex-specific differentiation trajectory (Figure 2C). These data confirm the previous report that sex determination occurs in supporting cells at E11.5 and is followed by the sexual differentiation of other cell types, including germ cells (Jameson et al., 2012). This observation is consistent with the previous reports that SRY activates SOX9 expression in supporting cells (Sekido et al., 2004), and these male supporting cells promote the male-type differentiation of surrounding cells and germ cells by secreting FGF9 (Bowles et al., 2010; Kim et al., 2006; Colvin et al., 2001; Jameson et al., 2012), whereas WNT4 and BMP2 expressed in female supporting cells, together with RA secreted from the mesonephros, act on germ cells to promote the female pathway (Miyauchi et al., 2017; Wu et al., 2016). Therefore, we concluded our scRNA-seq data to be sufficiently reliable to analyze the sexual differentiation of each cell type.

The expression pattern of sex-specific genes

As we focused on germ cell properties, we evaluated the data quality by extracting the germ cell population. We examined early sexual differentiation pathways by the expression of marker genes, *Lefty1*, *Lefty2*, *Nanos2*, and *Dnmt3l* for the male cascade (Wu et al., 2013; Tsuda et al., 2003; Sakai et al., 2004), and *Zglp1*, *Stra8*, *Rec8*, and *Figla* for the female cascade (Nagaoka et al., 2020; Menke et al., 2003; Bannister et al., 2004; Liang et al., 1997) (Figure S7). *Lefty1* and *Lefty2* expression increased at E12.5, that of *Nanos2* increased at E13.5 and that of *Dnmt3l* increased at E15.5 in mostly in males, whereas the increase in expression of *Zglp1*, *Stra8*, and *Rec8* (from E12.5) and *Figla* (from E13.5) occurred mostly in females. These data support our germ cell data being useful to analyze the sex-specific differentiation events.

Cell cycle changes during the differentiation of germ cells

To characterize the cell cycle state of each germ cell, we conducted cell cycle analysis using a previously reported method (Macosko et al., 2015; Kashima et al., 2018). As germ cells have a specific cell cycle phase, meiosis, we further modified the method to apply to germ cells (see STAR Methods for details). This method enabled the visualization of each cell cycle state during germ cell differentiation. As expected, most germ cells were mitotically active at early stages (E11.5 and E12.5) (Figure 3A). After segregation into a sex-specific direction, cell cycle states demonstrated sex specificity. In the female trajectory, meiotic cells accumulated from E13.5 and reached almost 100% at E15.5. In the male trajectory, unclassified cells accumulated from E13.5 and most cells were assigned as unclassified at E14.5 (Figures 3A and 3B). E13.5 is the time point when the cells enter G0 arrest (Western et al., 2008); therefore, we considered these unclassified cells to mainly consist of G0 arrested cells (hereafter we call this group G0). This is consistent with previous reports (Western et al., 2008; Miles et al., 2010), supporting the use of our scRNA-seq data to analyze cell cycle regulation during germ cell development.

Nanos2 expression precedes cell cycle arrest

As shown in Figure 1D, NANOS2 expression may precede mitotic arrest. To validate this observation using scRNA-seq data, we examined the relationship between *Nanos2* expression and the cell cycle in detail. *Nanos2* expression was detected mostly in male germ cells at E13.5 and E14.5 (Figure 3C). To correlate *Nanos2* expression with the cell cycle status, we measured *Nanos2* expression levels in each cell cycle state at E13.5 (Figures 3D–3F). *Nanos2* expression was not detected in G1 or G1/S but was noted in G2/M/G-phase cells at E13.5, and when *Nanos2* expression peaked, G0 population accumulated (Figure 3F). This

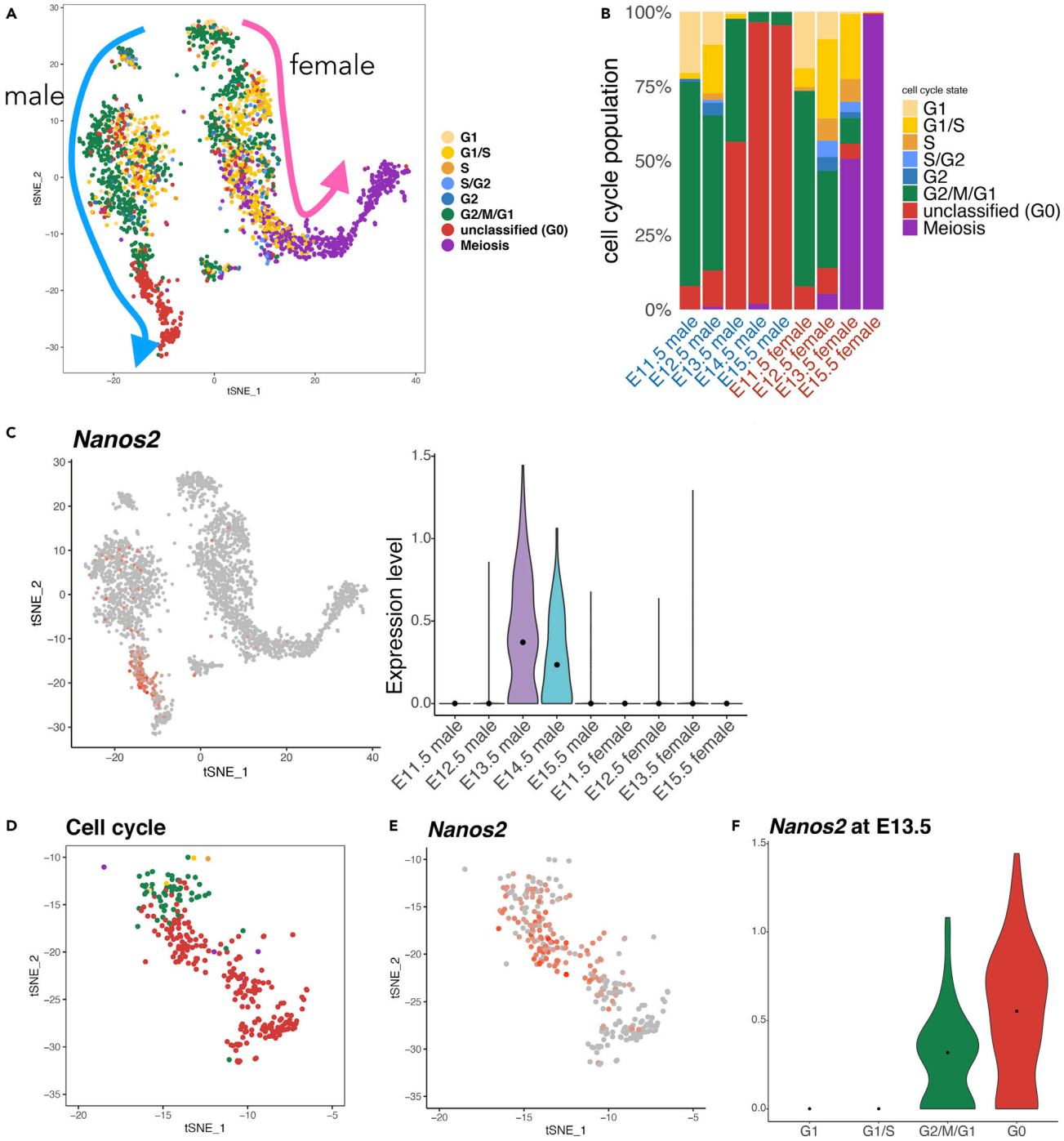

Figure 3. Relationship between cell cycle arrest and *Nanos2* expression

(A and B) Cell cycle estimation of germ cells. (A) shows the tSNE plot for germ cells. Cells are colored by the estimated cell cycle phase. Differentiation directions estimated by embryonic stage and sex of each cell (refer to Figure 2C) are indicated as arrows. The quantified data are shown in (B).

(C) Relative expression of *Nanos2* is shown. Cells with high expression are colored darker red. Violin plot on the right panel shows *Nanos2* expression. Black dots indicate the median in each stage.

(D) An enlarged tSNE plot to focus on E13.5-E15.5 male germ cells. Cells are colored by the estimated cell cycle stage.

(E) Relative expression of *Nanos2* is visualized on the tSNE plot of (D).

(F) Violin plot for *Nanos2* expression at E13.5 in each cycle phase. Black dots indicate the median in each phase.

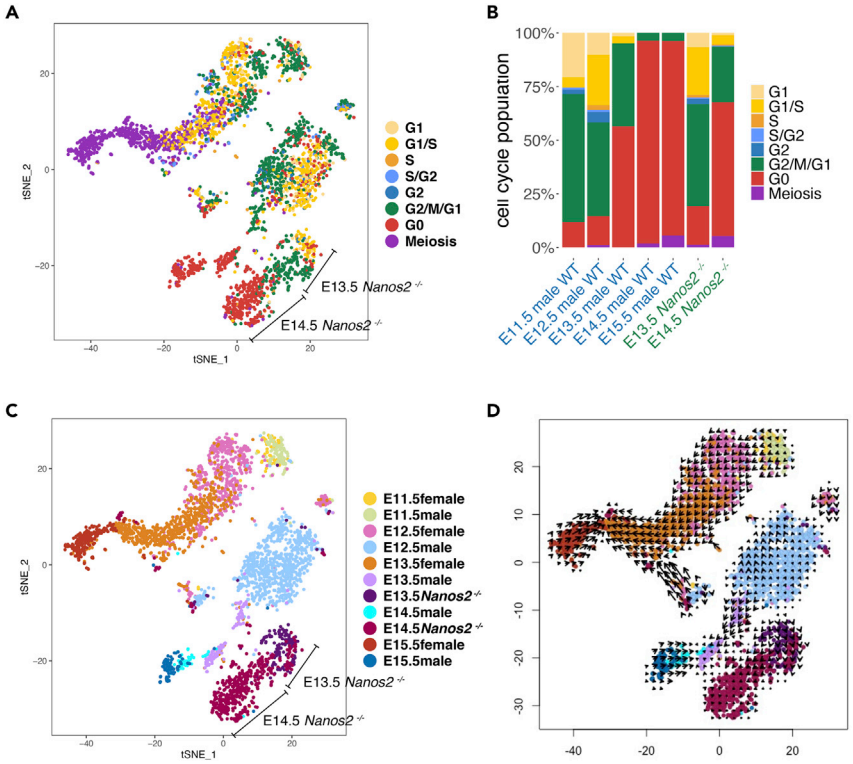

Figure 4. NANOS2 is required for the initiation of cell cycle arrest

(A–D) tSNE plot for wild-type and *Nanos2* $^{-/-}$ germ cells. Cells are colored by cell cycle phase in (A), and embrynic stage and genotype in (C). The quantified data (A) are shown in (B). (D) RNA velocity was projected on the tSNE plot. Arrows indicate directions of cell differentiation, and the strength was estimated by the expression profile of spliced and unspliced forms of RNAs.

correlation was also visualized by pseudo-time analysis (Figure S8). These data suggest that *Nanos2* expression starts before cells enter an arrested state. Although *Nanos2* mRNA expression declines after E14.5 (Figure 3E), NANOS2 protein exists for a longer period (Suzuki et al., 2016). Therefore, the arrested state of the cell cycle can be maintained by NANOS2. These results are consistent with FACS analysis (Figure 1D), which prompted us to further investigate the importance of NANOS2 for the induction of cell cycle arrest.

Cell cycle regulation in *Nanos2*$^{-/-}$ cells

If NANOS2 is involved in the induction of cell cycle arrest, *Nanos2*$^{-/-}$ germ cells should fail to enter mitotic arrest. On the other hand, our cell spreading experiment, shown in Figure 1C, and previous immunostaining (Suzuki and Saga 2008; Saba et al., 2014a) revealed that a substantial proportion of *Nanos2*$^{-/-}$ germ cells are negative for cell cycle markers. To clarify this contradiction, we next performed scRNA-seq using *Nanos2*$^{-/-}$ testes at E13.5 and E14.5 to analyze cell cycle states in *Nanos2*$^{-/-}$ germ cells. We re-performed cell cycle analyses by including scRNA-seq data of *Nanos2*$^{-/-}$ germ cells. More than 80% of *Nanos2*$^{-/-}$germ cells at E13.5 were not categorized as G0, similar to wild-type male germ cells at E12.5 (Figures 4A and 4B). This suggests that *Nanos2*$^{-/-}$ germ cells failed to enter the arrested stage at E13.5. However, approximately 70% of *Nanos2*$^{-/-}$ cells were assigned to G0 at E14.5 (Figure 4B), being consistent with previous reports (Suzuki and Saga 2008; Saba et al., 2014a) and implying that NANOS2-independent mechanisms also function to repress cell cycle progression in male germ cells. Consistent with these cell cycle changes in *Nanos2*$^{-/-}$ germ cells, gene enrichment analysis demonstrated cell cycle-related genes to be highly upregulated in *Nanos2*$^{-/-}$ germ cells at E13.5; however, these terms were not listed at E14.5 (Figure S9, Tables S1 and S2). We previously reported that RB function is active at E14.5 but not at E15.5 in *Nanos2*$^{-/-}$ (Saba et al., 2014a). This suggests that NANOS2 expression is required to repress the cell cycle at E13.5, but there are other mechanisms, such as RB regulation, to compensate for or function in parallel with NANOS2 for complete repression of the cell cycle.

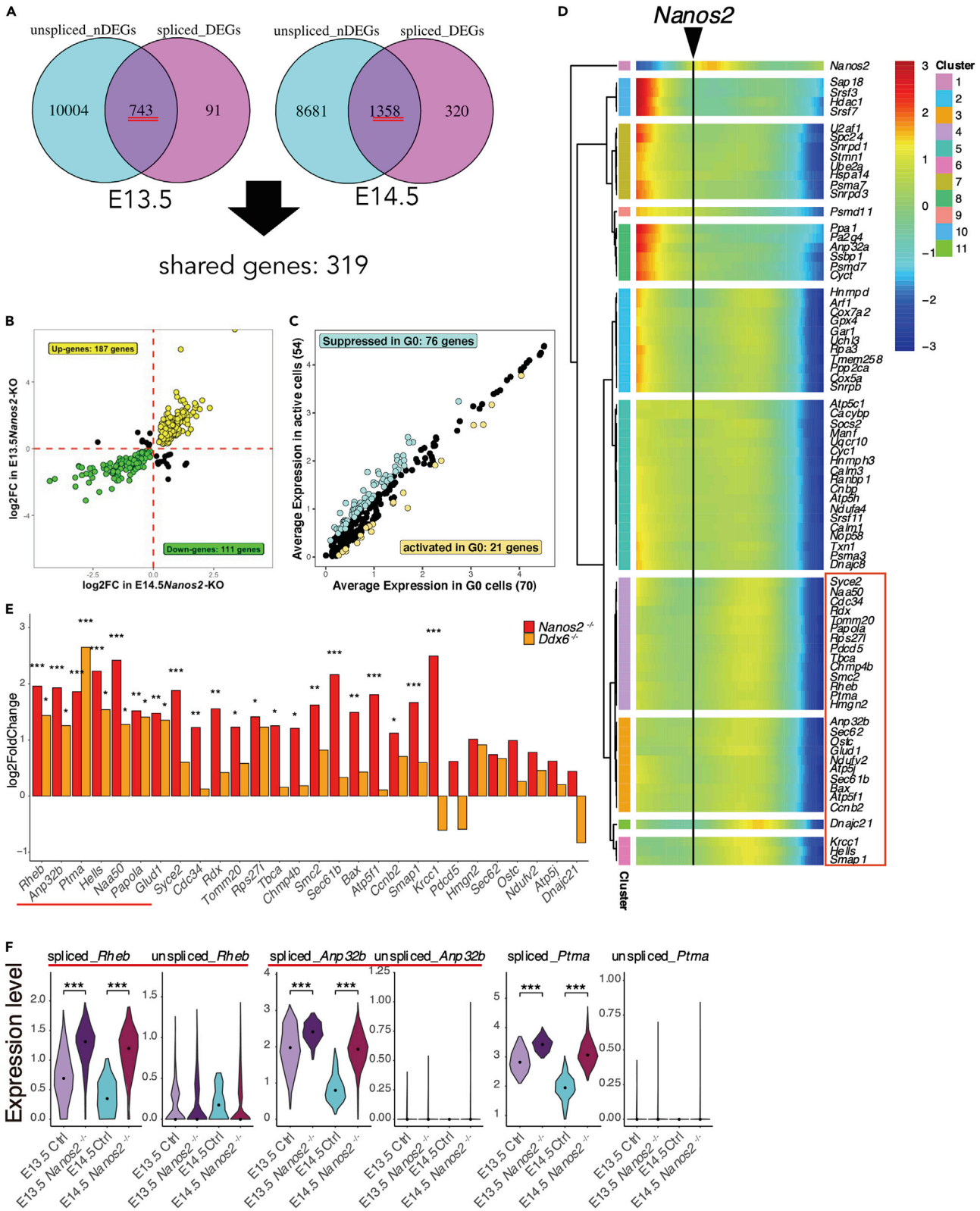
A
unspliced_nDEGs
spliced_DEGs
10004
743
91
E13.5
unspliced_nDEGs
spliced_DEGs
8681
1358
320
E14.5
shared genes: 319
B
Up-genes: 187 genes
Down-genes: 111 genes
log2FC in E13.5Nanos2-KO
log2FC in E14.5Nanos2-KO
C
Suppressed in G0: 76 genes
activated in G0: 21 genes
Average Expression in active cells (54)
Average Expression in G0 cells (70)
D
Nanos2
Cluster
E
Nanos2 -/-
Ddx6 -/-
log2FoldChange
Rheb
Anp32b
Ptma
Hells
Naa50
Papola
Glud1
Syce2
Cdc34
Rdx
Tomm20
Rps27l
Tbca
Chmp4b
Smc2
Sec61b
Bax
Atp5f1
Ccnb2
Smap1
Krcc1
Pdcd5
Hmgn2
Sec62
Ostc
Ndufv2
Atp5j
Dnajc21
F
spliced_Rheb
unspliced_Rheb
spliced_Anp32b
unspliced_Anp32b
spliced_Ptma
unspliced_Ptma
Expression level
E13.5 Ctrl
E13.5 Nanos2 -/-
E14.5 Ctrl
E14.5 Nanos2 -/-

Figure 5. Identification of target gene candidates suppressed by NANOS2

(A) Venn diagrams comparing nDEGs of unspliced forms and DEGs of spliced forms in *Nanos2* $^{-/-}$ germ cells at E13.5 (left) and E14.5 (right). In total, 743 and 1,358 genes were listed as spliced form-specific DEGs in E13.5 and E14.5, respectively, and 319 genes were shared.

(B) The scatterplot to compare the log2 fold change in *Nanos2* $^{-/-}$ samples at E13.5 (y axis) and E14.5 (x axis). Upregulated genes in the KO both at E13.5 and E14.5 (Up-genes) are colored in yellow and downregulated genes in the KO (Down-genes) are colored in green. Red dashed lines were drawn at 0.

(C) The gene expression of 187 upregulated genes identified in (B) in G0 arrested (x axis) and mitotic (y axis) male germ cells at E13.5 is shown. Average expression levels were calculated for each condition and plotted. Light blue dots were suppressed and orange dots were activated in G0 cells. The number of cells used for average calculation is indicated in parentheses on each axis.

(D) The gene expression patterns of the 76 obtained gene candidates suppressed by NANOS2 along the developmental pseudo-time of male germ cells. The point when *Nanos2* expression started is indicated as a vertical line. Genes surrounded by a red rectangle exhibited downregulation just after *Nanos2* expression.

(E) The expression changes of identified genes in (D) in *Nanos2* $^{-/-}$ (red) and *Ddx6* $^{-/-}$ (orange) male germ cells at E16.5. The log2 fold changes are shown as bar graph. The red under line indicates differentially expressed genes in both *Nanos2*$^{-/-}$ and *Ddx6*$^{-/-}$. ***p < 0.001, **p < 0.01 and *p < 0.05 (Wald test).

(F) The expression changes of NANOS2 target candidates, *Rheb*, *Anp32b*, and *Ptma*, which showed significant changes only in the spliced form at E13.5 and E14.5. Red underlines indicate mTORC1-related genes (see Figure 6 for details). Black dots indicate the median. ***p < 0.001 (Wilcoxon rank-sum test). The p value for each spliced and unspliced transcripts are as follows; *Rheb* 5.83×10^{-25} (E13.5, spliced), 0.958 (E13.5, unspliced), 5.01×10^{-28} (E14.5, spliced), and 0.0842 (E14.5, unspliced); *Anp32b* 1.51×10^{-12} (E13.5, spliced), 0.939 (E13.5, unspliced), and 3.97×10^{-29} (E14.5, spliced), 0.309 (E14.5, unspliced) and *Ptma* 2.96-30 (E13.5, spliced), 0.0630 (E13.5, unspliced), 3.97×10^{-29} (E14.5, spliced), and 0.110 (E14.5, unspliced).

As *Nanos2*$^{-/-}$ cells exhibited meiotic marker gene expression, such as STRA8 and SYCP3 (Suzuki and Saga 2008), which are widely used as female markers at embryonic stages, we expected *Nanos2*$^{-/-}$ male germ cells to be plotted closer to the wild-type female trajectory. However, *Nanos2*$^{-/-}$ germ cells were plotted to the male side, indicating that these cells retained male properties (Figure 4C). The UMAP plot yielded the same result (Figure S10). To examine the cell fate of *Nanos2*$^{-/-}$ germ cells, we conducted RNA velocity analysis, which estimates the future cell fate by analyzing unspliced nascent RNAs, enabling visualization of the direction and strength of differentiation (La Manno et al., 2018). This analysis supported the idea that *Nanos2*$^{-/-}$ germ cells are not feminized because the arrows of each mutant germ cell did not point to the female side (Figure 4D).

Identification of NANOS2 targets involved in regulation of the cell cycle

We assume that NANOS2 targets are recognized by both NANOS2 and DND1 but not only by DND1 because the recognition motif of DND1 is U-rich sequences, which are observed in many transcripts (Yamaji et al., 2017). Therefore, to understand the mechanism of NANOS2-mediated cell cycle arrest, it is important to identify the NANOS2 targets involved in cell cycle regulation. As NANOS2 localizes only in the cytoplasm, we expected NANOS2 to suppress spliced transcripts but not unspliced transcripts (Figure S11A). Therefore, we focused on genes exhibiting expression changes only in spliced transcripts to identify possible direct targets of NANOS2. For this purpose, we examined gene expression changes in spliced and unspliced transcripts separately using our scRNA-seq data. To analyze the expression changes of unspliced transcripts, we calculated the expression value of unspliced transcripts from UMI counts, which were counted during the estimation of RNA velocity (see STAR Methods for details). We first identified differentially expressed genes (DEGs) of spliced transcripts in *Nanos2*$^{-/-}$ male germ cells at E13.5 and E14.5 and extracted 834 and 1,678 DEGs, respectively (Tables S3 and S4). This population also contained transcriptionally regulated genes. To obtain only post-transcriptionally regulated genes, we selected genes without expression changes in unspliced transcripts (nDEGs). As the number of UMIs for unspliced transcripts was limited (Figure S12), most genes were identified as unchanged. However, we identified 743 and 1,358 gene candidates at E13.5 and E14.5, respectively, and 319 genes were shared between gene lists (Figure 5A and Table S5). Among 319 shared genes, 187 and 111 were consistently up- or downregulated in *Nanos2*$^{-/-}$ germ cells between E13.5 and E14.5 (Figure 5B and Table S6).

To identify gene candidates involved in cell cycle arrest, we searched for genes exhibiting expression differences between G0 (arrested) and mitotically active cells at E13.5 in wild-type male germ cells. Among 187 upregulated genes in *Nanos2*$^{-/-}$ germ cells, 76 were suppressed in wild-type arrested cells, and among 111 downregulated genes, 21 were activated in wild-type arrested cells (Figure 5C and Table S9). We reasoned that NANOS2 target genes exhibit correlated gene expression changes with *Nanos2* expression during male germ cell differentiation. Thus, we conducted pseudo-time analysis for the obtained gene candidates (Trapnell et al., 2014; Qiu et al., 2017a). In this analysis, male germ cells were aligned to make a single-direction trajectory, enabling gene expression changes along cell differentiation to be visualized (Figure 5D). By selecting genes exhibiting expression changes just after *Nanos2* expression, we obtained 25 and 7 genes as candidates being suppressed and activated by NANOS2, respectively

(Figures 5D and S13). As the main function of NANOS2 is the suppression of target genes, we further focused on the 25 suppressed candidates.

To identify more reliable targets, we used our previous data set obtained from *Ddx6*-KO germ cells (Shimada et al., 2019). NANOS2 and DDX6 colocalize to processing bodies in which RNA may be suppressed. As NANOS2 suppresses the cell cycle in a DDX6-dependent manner (Shimada et al., 2019), we expected commonly upregulated genes in both *Nanos2*$^{-/-}$ and *Ddx6*$^{-/-}$ germ cells include candidates involved in cell cycle regulation. To obtain such genes, we re-purposed RNA-seq data obtained from E16.5 in *Nanos2*$^{-/-}$ and *Ddx6*$^{-/-}$ germ cells (Shimada et al., 2019). We found 7 genes, *Rheb*, *Anp32b*, *Ptma*, *Hells*, *Naa50*, *Papola,* and *Glud1,* whose expression was significantly upregulated in both *Nanos2*$^{-/-}$ and *Ddx6*$^{-/-}$ germ cells (Figure 5E). Among them, only spliced transcripts of *Rheb*, *Anp32b,* and *Ptma* were upregulated in *Nanos2*$^{-/-}$ germ cells (Figures 5F and S11B). Importantly, all 3 genes are involved in cell proliferation (Bianco and Montano 2002; Vareli et al., 1996; Sun et al., 2001; Yang et al., 2016; Hao et al., 2018; Sancak et al., 2008). We concluded these 3 genes to be strong candidates of NANOS2 targets involved in cell cycle regulation.

NANOS2 directly suppresses target candidates in cultured cells

NANOS2 was reported to repress mTORC1 activity in spermatogonial stem cells (Zhou et al., 2015), and RHEB is an activator of mTORC1 (Sancak et al., 2008; Hao et al., 2018). In addition, Akt can activate mTORC1 via the inhibition of TSC function and ANP32B is known to activate Akt (Skeen et al., 2006; Inoki et al., 2002; Yang et al., 2016) (Figure 6A). Therefore, we expected that NANOS2 suppresses mTORC1 activity via the suppression of *Rheb* and *Anp32b,* and this repression may function in cell cycle arrest. To test this possibility, we first examined mTORC1 activity using phosphorylated ribosomal protein S6 signals (pS6), a key output of mTORC1 signaling, and Ki67 as a marker of the active cell cycle in *Nanos2*$^{+/-}$ and *Nanos2*$^{-/-}$ testes. In *Nanos2*$^{+/-}$ testes, no germ cells exhibited positive signals for pS6 or Ki67 at E15.5. In contrast, approximately 15% of *Nanos2*$^{-/-}$ germ cells had strong pS6 signals (Figure 6B), confirming that mTORC1 signaling was suppressed under the control of NANOS2. Among the pS6-positive germ cells, approximately 65% exhibited Ki67 signals, whereas only 9% of pS6-negative cells had Ki67 signals (Figure 6B), suggesting a strong correlation between cell cycle progression and mTORC1 activity in male germ cells.

Next, we conducted RNA-IP analysis to assess whether NANOS2 directly regulates these candidate mRNAs. As the germ cell number is limited in the testes, we utilized a cultured cell system with NIH3T3 cells developed in our laboratory in which cell cycle arrest can be induced upon doxycycline (Dox)-inducible NANOS2 and DND1 expression. In this system, 3xFlag-tagged NANOS2 and its essential partner, HA-tagged DND1, are induced by the addition of Dox, and NANOS2 target RNAs should be co-precipitated using anti-FLAG antibody. We confirmed that DND1 was co-precipitated with NANOS2 by anti-FLAG antibody (Figure S14A) and all three genes, *Anp32b*, *Rheb,* and *Ptma* are expressed in NIH3T3 cells according to scRNA-seq data (the data were downloaded from the homepage of 10 x Genomics) (Figure S14B). Therefore, we reasoned that NANOS2 expressed in cultured cells can interact with endogenously expressed mRNA. We used *Actb* as a negative control. Although *Actb* may be bound by DND1 (Yamaji et al.), it was not precipitated or repressed by NANOS2-DND1. Co-precipitated RNAs were quantified by RT-qPCR. Compared with the negative control *Actb*, *Rheb,* and *Ptma* were enriched in the IP sample (Figure 6C), indicating that *Rheb* and *Ptma* are possible direct targets of NANOS2.

Lastly, to examine the effects of NANOS2 on the bound RNAs, we conducted NANOS2 functional analyses using this cultured cell system. We previously reported that NANOS2 regulates *Dazl* expression by binding to its 3′UTR (Kato et al., 2016). Thus, we expected these candidates to also be regulated through the binding of NANOS2 to their 3′UTR. We cloned the 3′UTR of gene candidates into a dual-fluorescence reporter vector (Figures S15A and S15B), in which mCherry serves as an internal control and EmGFP reports the activity of the 3′UTR of target RNAs. In the absence of NANOS2 and DND1 (DMSO treatment), EmGFP containing the candidate 3′UTR did not exhibit significant expression reduction compared with *Actb* control 3′UTR (Figure S15C). In contrast, in Dox-treated cells, all constructs (containing the 3′-UTR of *Rheb*, *Ptma,* or *Anp32b*) exhibited significant downregulation comparable with the repression level of the *Dazl* 3′UTR (Figure 6D), suggesting that NANOS2 suppresses the expression of these genes in a 3′UTR-dependent manner.

DISCUSSION

Arrest of the cell cycle is known as the first step of male-type differentiation in germ cells. It was previously suggested that NANOS2 represses *Dazl* to maintain cell cycle arrest by regulating RA responsiveness (Kato

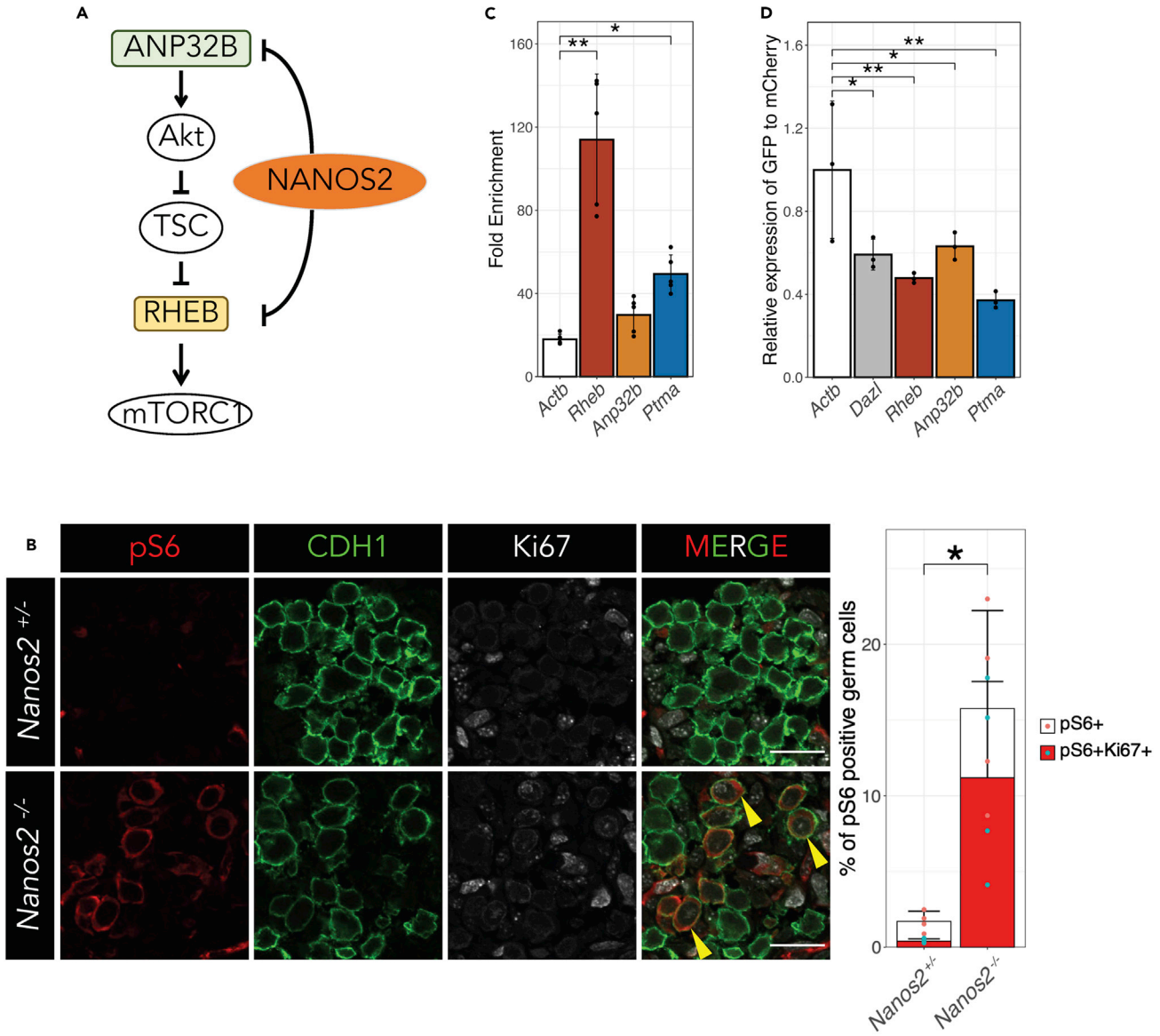

Figure 6. NANOS2 suppresses mTORC1 activity via the suppression of its activators

(A) A scheme of the regulatory pathway for mTORC1 activation. ANP32B and RHEB can activate mTORC1, and their mRNA expression is suppressed under the control of NANOS2 in male germ cells.

(B) Immunofluorescence analyses of testes from *Nanos2*$^{+/-}$ and *Nanos2* $^{-/-}$ at E15.5 using the active mTORC1 marker pS6, germ cell marker CDH1 and active cell cycle marker Ki67. Yellow arrowheads indicate pS6 and Ki67 double-positive cells. The quantified bar plot is shown on the right. White indicates the total population of pS6-positive germ cells and red indicates pS6 and Ki67 double-positive germ cells. Four independently prepared samples were analyzed. *$p < 0.05$ (t test). Scale bar = 20 μm

(C) RNA-IP experiments conducted using the cell culture system (see STAR Methods for details). Data are represented as mean with SD. The endogenous mRNAs were detected using RT-qPCR. n = 5. **$p < 0.01$ and *$p < 0.05$ (Dunnett's test).

(D) The relative expression value of *Emgfp* is shown. The *Emgfp* value was normalized by the *mCherry* value, and the relative value to the *Actb* 3′UTR was calculated. Data are represented as mean with SD. **$p < 0.01$ and *$p < 0.05$ (Dunnett's test).

et al., 2016). However, we revealed that *Dazl* is not the sole target of NANOS2 to stop the cell cycle, and scRNA-seq confirmed that NANOS2 plays a role in both the maintenance and initiation of cell cycle arrest. In this regard, we identified additional targets, *Rheb* and *Anp32b*, which function in the mTORC pathway separately from DAZL (Figure 7). Although *Anp32b* was not significantly enriched in the IP sample, it exhibited spliced form-specific expression changes in *Nanos2*$^{-/-}$ cells (Figure 5) and 3′UTR-dependent

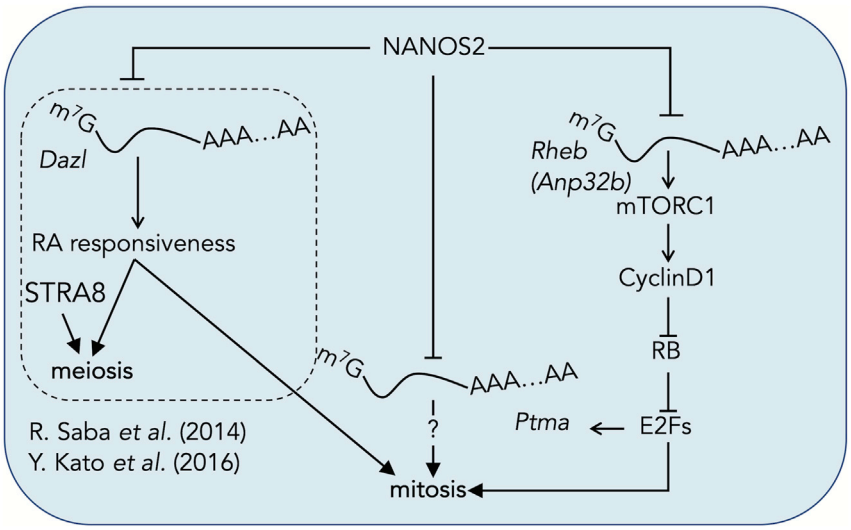

Figure 7. Gene network for cell cycle regulation during male germ cell development

Schematic drawing of the model proposed in this and previous studies. In the absence of NANOS2, DAZL, and STRA8 are upregulated and both mitotic and meiotic pathways are promoted. *Dazl* was identified as the direct target of NANOS2 and DAZL may increase RA responsiveness. The forced expression of DAZL promotes both mitotic and meiotic pathways (Kato et al., 2016). Double KO of NANOS2 and STRA8 represses only the meiotic pathway not the mitotic pathway (Saba et al., 2014a). Our dKO study revealed that *Dazl* is not the sole target of NANOS2 responsible for cell cycle regulation. NANOS2 also downregulates mTORC1 activity via the suppression of its activator(s), *Rheb*, *Amp32b*. This results in the downregulation of CyclinD1 and activates RB1, which suppresses E2F function. As an independent pathway, NANOS2 may also suppress *Ptma*.

downregulation by NANOS2 (Figure 6D), suggesting that it is recruited to P-bodies by other mechanisms and repressed in a similar manner to NANOS2 targets. NANOS2 was previously reported to suppress mTORC1 activity by anchoring MTOR protein in P-bodies in spermatogonial stem cells (Zhou et al., 2015). This report and our current study suggest that NANOS2 can regulate mTORC1 activity in multiple ways. However, we observed positivity of the active mTORC1 marker pS6 in some *Nanos2*$^{-/-}$ germ cells. Thus, there may be another pathway to mediate the effects of NANOS2. As one candidate, we identified *Ptma* as a NANOS2 target. PTMA is ubiquitously expressed in mice (Eschenfeldt and Berger 1986) and its expression is regulated by E2Fs (Vareli et al., 1996). Inhibition of *Ptma* by antisense oligomers prevents cell division (Sburlati et al., 1991). As mTORC1 activity promotes Cyclin D1 protein expression (Averous et al., 2008), which activates E2F function via the inhibition of RB1 (Resnitzky and Reed 1995), *Ptma* may be suppressed both transcriptionally (mTORC1-dependent) and post-transcriptionally (mTORC1-independent) under the control of NANOS2. PTMA expression peaks at around the late S or G2 phase (Vareli et al., 1996); therefore, it is expected to function at these cell cycle phases. Taken together, NANOS2 may regulate different cell cycle regulatory machineries at different cell cycle phases to effectively suppress the cell cycle (Figure 7).

Our study also suggested that a NANOS2-independent mechanism suppresses the cell cycle (Figures 4A and 4B). In our previous report, p38 MAPK signaling was identified as a NANOS2-independent pathway to suppress RA signaling (Wu et al., 2015). The p38 MAPK pathway is activated by numerous extracellular stimuli and is considered to lead to mitotic arrest in male germ cells (Ewen et al., 2010). Although we were unable to demonstrate a relationship between NANOS2 and p38 MAPK, it is a candidate cascade to suppress the cell cycle in parallel with NANOS2.

In addition to cell cycle regulation, NANOS2 represses meiotic initiation by repressing STRA8, keeps germ cells in the seminiferous tubules and, importantly, promotes male-type gene expression (Saba et al., 2014a; Suzuki and Saga 2008). We believe that other NANOS2 targets function in these important events. Based on our pseudo-time expression data, many other genes are downregulated just after *Nanos2* expression. However, there may not be a single responsible gene, as demonstrated for cell cycle regulation, which makes further functional analyses difficult.

Apart from NANOS2 function, our scRNA-seq data are useful to analyze the sex determination mechanism of germ cells occurring between E11.5 and E12.5 in male gonads. Although the genetic cascades leading to the sexual differentiation of somatic cells are well studied, somatic factors to induce male germ cell determination have not been identified. As our data include whole gonad information and we confirmed that sexual differentiation starts earlier in supporting cells than in germ cells (Figure 2C), further studies focusing on the signal transduction pathways are expected to clarify causative reciprocal interactions.

Although we focused only on genes repressed by NANOS2 associated with cell cycle arrest in this study, scRNA-seq identified many genes that are upregulated following NANOS2 expression. As the major function of NANOS2 is considered to be the repression of gene expression, such upregulation may be a secondary effect. Further functional analyses will delineate a gene network by which male germ cell differentiation is orchestrated.

Limitations of the study

By the analysis of single-cell RNA-seq data, we concluded that NANOS2 acts as a potent cell cycle repressor. Although we identified possible target RNAs that could suppress mTORC1 pathway leading to cell cycle arrest, the functional relevancy is still unknown. Since NANOS2 may suppress many RNAs together, it would be difficult to clarify the cause of phenotype by focusing single gene. In addition, the function of NANOS2 is not limited for repressing cell cycle. NANOS2 is a major male promoting factor, but the mechanism is currently unknown. The identification of key targets of NANOS2 and decoding those contributions to each phenotype are critically important to understand the mechanism of male-type differentiation of germ cells in mammal.

Materials and data availability

All unique/stable reagents generated in this study are available from the lead contact with a completed Materials and Transfer Agreement.

The scRNA-seq data generated during this study are included in this article (and its supplementary information files). Sequence data were deposited in the DNA Data Bank of Japan: DRA011172.

STAR★METHODS

Detailed methods are provided in the online version of this paper and include the following:

- KEY RESOURCES TABLE
- RESOURCE AVAILABILITY
  - Lead contact
  - Materials availability
  - Data availability
- EXPERIMENTAL MODEL AND SUBJECT DETAILS
  - Animals
  - Cell lines
- METHOD DETAILS
  - Preparation of germ cell spreads
  - Gonad sample preparation and immunostaining
  - Flow cytometry
  - Single-cell RNA-seq
  - RNA immunoprecipitation and reverse-transcription quantitative PCR
  - Functional assessment of 3'UTR using the dual reporter system
- QUANTIFICATION AND STATISTICAL ANALYSIS
  - Statistical analysis was performed using R.
  - Statistical analysis of scRNA-seq
  - Cell cycle analysis of germ cells
  - Identification of post-transcriptionally regulated gene candidates
  - Gene enrichment analysis
  - RNA-seq re-analysis

SUPPLEMENTAL INFORMATION

Supplemental information can be found online at https://doi.org/10.1016/j.isci.2021.102890.

ACKNOWLEDGMENTS

We thank Drs K. Ishiguro for the anti-REC8 antibody, S. Yamanaka for the anti-DNMT3L antibody, Y. Nishimune for the anti-GCNA antibody, A. Suzuki for the *Oct4dPE-CreER^{t2}*mouse line and anti-DND1 antibody, Mr. M. Muraoka for his kind support in establishing the analysis environment for chromium data and Dr. Danelle Wright for editing this manuscript. We also thank for Dr. A. Toyoda for his kind support to prepare the chromium library and sequencing. This study was partly supported by Japan Society for Promotion of Science KAKENHI Grant Numbers 16H06279, 25112002, 26251025 and 17H06166 to Y.S., and 18J12483 to R.S.

AUTHOR CONTRIBUTIONS

All experiments except for cell spread staining analysis (conducted by H.K.) were conducted by R.S. The ciN2D1-3T3 cell line was established by T.H. The manuscript was written by R.S. and Y.S. The revised manuscript was written by R.S., Y.K., and Y.S.

DECLARATION OF INTERESTS

The authors declare no competing interests.

Received: October 13, 2020
Revised: June 15, 2021
Accepted: July 16, 2021
Published: August 20, 2021

REFERENCES

Anderson, E.L., Baltus, A.E., Roepers-Gajadien, H.L., Hassold, T.J., de Rooij, D.G., van Pelt, A.M.M., and Page, D.C. (2008). Stra8 and its inducer, retinoic acid, regulate meiotic initiation in both spermatogenesis and oogenesis in mice. Proc. Natl. Acad. Sci. U S A *105*, 14976–14980.

Anderson, R., Copeland, T.K., Schöler, H., Heasman, J., and Wylie, C. (2000). The onset of germ cell migration in the mouse embryo. Mech. Dev. *91*, 61–68.

Averous, J., Fonseca, B.D., and Proud, C.G. (2008). Regulation of cyclin D1 expression by mTORC1 signaling requires eukaryotic initiation factor 4E-binding protein 1. Oncogene *27*, 1106–1113.

Bannister, L.A., Reinholdt, L.G., Munroe, R.J., and Schimenti, J.C. (2004). Positional cloning and characterization of mousemei8, a disrupted allele of the meiotic cohesinRec8. Genesis *40*, 184–194.

Bianco, N.R., and Montano, M.M. (2002). Regulation of prothymosin α by estrogen receptor α: Molecular mechanisms and relevance in estrogen-mediated breast cell growth. Oncogene *21*, 5233–5244.

Bowles, J., Feng, C.W., Spiller, C., Davidson, T.L., Jackson, A., and Koopman, P. (2010). FGF9 suppresses meiosis and promotes male germ cell fate in mice. Dev. Cell *19*, 440–449.

Bowles, J., Knight, D., Smith, C., Wilhelm, D., Richman, J., Mamiya, S., Yashiro, K., Chawengsaksophak, K., Wilson, M.J., Rossant, J., et al. (2006). Retinoid signaling determines germ cell fate in mice. Science *312*, 596–600.

Butler, A., Hoffman, P., Smibert, P., Papalexi, E., and Satija, R. (2018). Integrating single-cell transcriptomic data across different conditions, technologies, and species. Nat. Biotechnol. *36*, 411–420.

Chuma, S., and Nakatsuji, N. (2001). Autonomous transition into meiosis of mouse fetal germ cells in vitro and its inhibition by gp130-mediated signaling. Dev. Biol. *229*, 468–479.

Colvin, J.S., Green, R.P., Schmahl, J., Capel, B., and Ornitz, D.M. (2001). Male-to-Female sex reversal in mice lacking fibroblast growth factor 9. Cell *104*, 875–889.

Decker, C.J., and Parker, R. (2012). P-bodies and stress granules: possible roles in the control of translation and mRNA degradation. Cold Spring Harb. Perspect. Biol. *4*, a012286.

Ellis, B., Haaland, P., Hahne, F., Meur, N. Le, Gopalakrishnan, N., Spidlen, J., Jiang, Fm, and Finak, G. (2019). flowCore: flowCore: Basic Structures for Flow Cytometry Data.

Eschenfeldt, W.H., and Berger, S.L. (1986). The human prothymosin alpha gene is polymorphic and induced upon growth stimulation: evidence using a cloned cDNA. Proc. Natl. Acad. Sci. U S A *83*, 9403–9407.

Ewen, K., Jackson, A., Wilhelm, D., and Koopman, P. (2010). A male-specific role for p38 mitogen-activated protein kinase in germ cell sex differentiation in Mice1. Biol. Reprod. *83*, 1005–1014.

Fukuda, K., Masuda, A., Naka, T., Suzuki, A., Kato, Y., and Saga, Y. (2018). Requirement of the 3′-UTR-dependent suppression of DAZL in oocytes for pre-implantation mouse developmentM.S. Bartolomei, ed. *14*, e1007436.

Gill, M.E., Hu, Y.C., Lin, Y., and Page, D.C. (2011). Licensing of gametogenesis, dependent on RNA binding protein DAZL, as a gateway to sexual differentiation of fetal germ cells. Proc. Natl. Acad. Sci. U S A *108*, 7443–7448.

Hao, F., Kondo, K., Itoh, T., Ikari, S., Nada, S., Okada, M., and Noda, T. (2018). Rheb localized on the Golgi membrane activates lysosome-localized mTORC1 at the Golgi-lysosome contact site. J. Cell Sci. *131*, jcs208017.

Hayashi-Takanaka, Y., Yamagata, K., Nozaki, N., and Kimura, H. (2009). Visualizing histone modifications in living cells: spatiotemporal dynamics of H3 phosphorylation during interphase. J. Cell Biol. *187*, 781–790.

Hayashi, K., de Sousa Lopes, S.M.C., and Surani, M.A. (2007). Germ cell specification in mice. Science *316*, 394–396.

Hothorn, T., Bretz, F., and Westfall, P. (2008). Simultaneous inference in general parametric models. Biomater. J. *50*, 346–363.

Inoki, K., Li, Y., Zhu, T., Wu, J., and Guan, K.L. (2002). TSC2 is phosphorylated and inhibited by Akt and suppresses mTOR signalling. Nat. Cell Biol. *4*, 648–657.

Ishiguro, K.I., Matsuura, K., Tani, N., Takeda, N., Usuki, S., Yamane, M., Sugimoto, M., Fujimura, S., Hosokawa, M., Chuma, S., et al. (2020). MEIOSIN directs the switch from mitosis to meiosis in

mammalian germ cells. Dev. Cell *52*, 429–445.e10.

Ishiguro, K.I., Kim, J., Fujiyama-Nakamura, S., Kato, S., and Watanabe, Y. (2011). A new meiosis-specific cohesin complex implicated in the cohesin code for homologous pairing. EMBO Rep. *12*, 267–275.

Jameson, S.A., Natarajan, A., Cool, J., DeFalco, T., Maatouk, D.M., Mork, L., Munger, S.C., and Capel, B. (2012). Temporal transcriptional profiling of somatic and germ cells reveals biased lineage priming of sexual fate in the fetal mouse gonadG.S. Barsh, ed. *8*, e1002575.

Kashima, Y., Suzuki, A., Liu, Y., Hosokawa, M., Matsunaga, H., Shirai, M., Arikawa, K., Sugano, S., Kohno, T., Takeyama, H., et al. (2018). Combinatory use of distinct single-cell RNA-seq analytical platforms reveals the heterogeneous transcriptome response. Sci. Rep. *8*, 3482.

Kato, Y., Katsuki, T., Kokubo, H., Masuda, A., and Saga, Y. (2016). Dazl is a target RNA suppressed by mammalian NANOS2 in sexually differentiating male germ cells. Nat. Commun. *7*, 11272.

Kim, Y., Kobayashi, A., Sekido, R., DiNapoli, L., Brennan, J., Chaboissier, M.-C., Poulat, F., Behringer, R.R., Lovell-Badge, R., and Capel, B. (2006). Fgf9 and Wnt4 act as antagonistic signals to regulate mammalian sex determinationH. Hamada, ed. *4*, e187.

Koubova, J., Menke, D.B., Zhou, Q., Capel, B., Griswold, M.D., and Page, D.C. (2006). Retinoic acid regulates sex-specific timing of meiotic initiation in mice. Proc. Natl. Acad. Sci. U S A *103*, 2474–2479.

La Manno, G., Soldatov, R., Zeisel, A., Braun, E., Hochgerner, H., Petukhov, V., Lidschreiber, K., Kastriti, M.E., Lönnerberg, P., Furlan, A., et al. (2018). RNA velocity of single cells. Nature *560*, 494–498.

Liang, L., Soyal, S.M., and Dean, J. (1997). FIGalpha, a Germ Cell Specific Transcription Factor Involved in the Coordinate Expression of the Zona Pellucida Genes (The Company of Biologists).

Love, M.I., Huber, W., and Anders, S. (2014). Moderated estimation of fold change and dispersion for RNA-seq data with DESeq2. Genome Biol. *15*, 550.

Macosko, E.Z., Basu, A., Satija, R., Nemesh, J., Shekhar, K., Goldman, M., Tirosh, I., Bialas, A.R., Kamitaki, N., Martersteck, E.M., et al. (2015). Highly parallel genome-wide expression profiling of individual cells using nanoliter droplets. Cell *161*, 1202–1214.

Menke, D.B., Koubova, J., and Page, D.C. (2003). Sexual differentiation of germ cells in XX mouse gonads occurs in an anterior-to-posterior wave. Dev. Biol. *262*, 303–312.

Miles, D.C., Van Den Bergen, J.A., Sinclair, A.H., and Western, P.S. (2010). Regulation of the female mouse germ cell cycle during entry into meiosis. Cell Cycle *9*, 408–418.

Miyauchi, H., Ohta, H., Nagaoka, S., Nakaki, F., Sasaki, K., Hayashi, K., Yabuta, Y., Nakamura, T., Yamamoto, T., and Saitou, M. (2017). Bone morphogenetic protein and retinoic acid synergistically specify female germ-cell fate in mice. EMBO J. *36*, 3100–3119.

Miyawaki, S., Kuroki, S., Ryo Maed, R., Okashita, N., Koopman, P., and Tachibana, M. (2020). The mouse Sry locus harbors a cryptic exon that is essential for male sex determination. Science *370*, 121–124.

Nagaoka, S.I., Nakaki, F., Miyauchi, H., Nosaka, Y., Ohta, H., Yabuta, Y., Kurimoto, K., Hayashi, K., Nakamura, T., Yamamoto, T., et al. (2020). ZGLP1 is a determinant for the oogenic fate in mice. Science *367*, eaaw4115.

Ono, K., and Han, J. (2000). The p38 signal transduction pathway Activation and function. Cell Signal. *12*, 1–13.

Parker, R., and Sheth, U. (2007). P bodies and the control of mRNA translation and degradation. Mol. Cell *25*, 635–646.

Qiu, X., Hill, A., Packer, J., Lin, D., Ma, Y.-A., and Trapnell, C. (2017a). Single-cell mRNA quantification and differential analysis with Census. Nat. Methods *14*, 309–315.

Qiu, X., Mao, Q., Tang, Y., Wang, L., Chawla, R., Pliner, H.A., and Trapnell, C. (2017b). Reversed graph embedding resolves complex single-cell trajectories. Nat. Methods *14*, 979–982.

R Core Team (2019). R: A Language and Environment for Statistical Computing (R Found Stat Comput).

Resnitzky, D., and Reed, S.I. (1995). Different roles for cyclins D1 and E in regulation of the G1-to-S transition. Mol. Cell. Biol. *15*, 3463–3469.

RStudio Team (2018). RStudio: Integrated Development for R (RStudio, Inc.).

Saba, R., Kato, Y., and Saga, Y. (2014a). NANOS2 promotes male germ cell development independent of meiosis suppression. Dev. Biol. *385*, 32–40.

Saba, R., Wu, Q., and Saga, Y. (2014b). CYP26B1 promotes male germ cell differentiation by suppressing STRA8-dependent meiotic and STRA8-independent mitotic pathways. Dev. Biol. *389*, 173–181.

Sakai, Y., Suetake, I., Shinozaki, F., Yamashina, S., and Tajima, S. (2004). Co-expression of de novo DNA methyltransferases Dnmt3a2 and Dnmt3L in gonocytes of mouse embryos. Gene Expr. Patterns *5*, 231–237.

Sancak, Y., Peterson, T.R., Shaul, Y.D., Lindquist, R.A., Thoreen, C.C., Bar-Peled, L., and Sabatini, D.M. (2008). The Rag GTPases bind raptor and mediate amino acid signaling to mTORC1. Science *320*, 1496–1501.

Sburlati, A.R., Manrow, R.E., and Berger, S.L. (1991). Prothymosin α antisense oligomers inhibit myeloma cell division. Proc. Natl. Acad. Sci. U S A *88*, 253–257.

Schindelin, J., Arganda-Carreras, I., Frise, E., Kaynig, V., Longair, M., Pietzsch, T., Preibisch, S., Rueden, C., Saalfeld, S., Schmid, B., et al. (2012). Fiji: an open-source platform for biological-image analysis. Nat. Methods *9*, 676–682.

Sekido, R., Bar, I., Narváez, V., Penny, G., and Lovell-Badge, R. (2004). SOX9 is up-regulated by the transient expression of SRY specifically in Sertoli cell precursors. Dev. Biol. *274*, 271–279.

Seligman, J., and Page, D.C. (1998). The Dazh gene is expressed in male and female embryonic gonads before germ cell sex differentiation. Biochem. Biophys. Res. Commun. *245*, 878–882.

Shimada, R., Kiso, M., and Saga, Y. (2019). ES-mediated chimera analysis revealed requirement of DDX6 for NANOS2 localization and function in mouse germ cells. Sci. Rep. *9*, 515.

Skeen, J.E., Bhaskar, P.T., Chen, C.C., Chen, W.S., Peng, X.D., Nogueira, V., Hahn-Windgassen, A., Kiyokawa, H., and Hay, N. (2006). Akt deficiency impairs normal cell proliferation and suppresses oncogenesis in a p53-independent and mTORC1-dependent manner. Cancer Cell *10*, 269–280.

Spiller, C.M., Wilhelm, D., and Koopman, P. (2010). Retinoblastoma 1 protein modulates XY germ cell entry into G1/G0 arrest during fetal development in Mice1. Biol. Reprod. *82*, 433–443.

Sun, W., Hattori, N., Mutai, H., Toyoshima, Y., Kimura, H., Tanaka, S., and Shiota, K. (2001). PAL31, a nuclear protein required for progression to the S phase. Biochem. Biophys. Res. Commun. *280*, 1048–1054.

Suzuki, A., Igarashi, K., Aisaki, K., Kanno, J., and Saga, Y. (2010). NANOS2 interacts with the CCR4-NOT deadenylation complex and leads to suppression of specific RNAs. Proc. Natl. Acad. Sci. *107*, 3594–3599.

Suzuki, A., Niimi, Y., Shinmyozu, K., Zhou, Z., Kiso, M., and Saga, Y. (2016). Dead end1 is an essential partner of NANOS2 for selective binding of target RNAs in male germ cell development. EMBO Rep. *17*, 37–46.

Suzuki, A., Saba, R., Miyoshi, K., Morita, Y., and Saga, Y. (2012). Interaction between NANOS2 and the CCR4-NOT deadenylation complex is essential for male germ cell development in mouseA.J. Cooney, ed. *7*, e33558.

Suzuki, A., and Saga, Y. (2008). Nanos2 suppresses meiosis and promotes male germ cell differentiation. Genes Dev. *22*, 430–435.

Suzuki, A., Tsuda, M., and Saga, Y. (2007). Functional redundancy among Nanos proteins and a distinct role of Nanos2 during male germ cell development. Development *134*, 77–83.

Tanaka, H., Pereira, Lavd, Nozaki, M., Tsuchida, J., Sawada, K., Mori, H., and Nishimune, Y. (1998). A germ cell-specific nuclear antigen recognized by a monoclonal antibody raised against mouse testicular germ cells. Int. J. Androl. *20*, 361–366.

Trapnell, C., Cacchiarelli, D., Grimsby, J., Pokharel, P., Li, S., Morse, M., Lennon, N.J., Livak, K.J., Mikkelsen, T.S., and Rinn, J.L. (2014). The dynamics and regulators of cell fate decisions are revealed by pseudotemporal ordering of single cells. Nat. Biotechnol. *32*, 381–386.

Tsuda, M., Sasaoka, Y., Kiso, M., Abe, K., Haraguchi, S., Kobayashi, S., and Saga, Y. (2003). Conserved role of nanos proteins in germ cell development. Science *301*, 1239–1241.

Van Rossum, G., and Drake, F.L. (2009). Python 3 Reference Manual.

Vareli, K., Tsolas, O., and Frangou-Lazaridis, M. (1996). Regulation of prothymosin alpha during the cell cycle. Eur. J. Biochem. *238*, 799–806.

Walter, W., Sánchez-Cabo, F., and Ricote, M. (2015). GOplot: an R package for visually combining expression data with functional analysis. Bioinformatics *31*, 2912–2914.

Western, P.S., Miles, D.C., van den Bergen, J.A., Burton, M., and Sinclair, A.H. (2008). Dynamic regulation of mitotic arrest in fetal male germ cells. Stem Cells *26*, 339–347.

Whitfield, M.L., Sherlock, G., Saldanha, A.J., Murray, J.I., Ball, C.A., Alexander, K.E., Matese, J.C., Perou, C.M., Hurt, M.M., Brown, P.O., et al. (2002). Identification of genes periodically expressed in the human cell cycle and their expression in tumorsM.J. Solomon, ed. *13*, 1977–2000.

Wright, D., Kiso, M., and Saga, Y. (2021). Genetic and structural analysis of the in vivo functional redundancy between murine NANOS2 and NANOS3. Development *148*, dev191916.

Wu, Q., Fukuda, K., Kato, Y., Zhou, Z., Deng, C.X., and Saga, Y. (2016). Sexual fate change of XX germ cells caused by the deletion of SMAD4 and STRA8 independent of somatic sex reprogrammingM.F. Wolfner, ed. *14*, e1002553.

Wu, Q., Fukuda, K., Weinstein, M., Graff, J.M., and Saga, Y. (2015). SMAD2 and p38 signaling pathways act in concert to determine XY primordial germ cell fate in mice. Development *142*, 575–586.

Wu, Q., Kanata, K., Saba, R., Deng, C.-X., Hamada, H., and Saga, Y. (2013). Nodal/activin signaling promotes male germ cell fate and suppresses female programming in somatic cells. Development *140*, 291–300.

Yamaji, M., Jishage, M., Meyer, C., Suryawanshi, H., Der, E., Yamaji, M., Garzia, A., Morozov, P., Manickavel, S., McFarland, H.L., et al. (2017). DND1 maintains germline stem cells via recruitment of the CCR4-NOT complex to target mRNAs. Nature *543*, 568–572.

Yang, S., Zhou, L., Reilly, P.T., Shen, S.M., He, P., Zhu, X.N., Li, C.X., Wang, L.S., Mak, T.W., Chen, G.Q., et al. (2016). ANP32B deficiency impairs proliferation and suppresses tumor progression by regulating AKT phosphorylation. Cell Death Dis. *7*, e2082.

Yao, H.H.C., Matzuk, M.M., Jorgez, C.J., Menke, D.B., Page, D.C., Swain, A., and Capel, B. (2004). Follistatin operates downstream of Wnt4 in mammalian ovary organogenesis. Dev. Dyn. *230*, 210–215.

Zacksenhaus, E., Jiang, Z., Chung, D., Marth, J.D., Phillips, R.A., and Gallic, B.L. (1996). pRb controls proliferation, differentiation, and death of skeletal muscle cells and other lineages during embryogenesis. Genes Dev. *10*, 3051–3064.

Zhou, Y., Zhou, B., Pache, L., Chang, M., Khodabakhshi, A.H., Tanaseichuk, O., Benner, C., and Chanda, S.K. (2019). Metascape provides a biologist-oriented resource for the analysis of systems-level datasets. Nat. Commun. *10*, 1523.

Zhou, Z., Shirakawa, T., Ohbo, K., Sada, A., Wu, Q., Hasegawa, K., Saba, R., and Saga, Y. (2015). RNA binding protein Nanos2 organizes post-transcriptional buffering system to retain primitive state of mouse spermatogonial stem cells. Dev. Cell *34*, 96–107.

STAR★METHODS

KEY RESOURCES TABLE

REAGENT or RESOURCE	SOURCE	IDENTIFIER
Antibodies		
Rat Anti-GCNA (IF, 1:4000)	A gift from Dr. Nishimune (Tanaka et al., 1998)	N/A
Rabbit Anti-REC8 (IF, 1:100)	A gift from Dr. Ishiguro (Ishiguro et al., 2011)	N/A
Mouse Anti-phospho-histone H3 (ser10)	A gift from Dr. Kimura (Hayashi-Takanaka et al., 2009)	N/A
Goat Anti-Human/Mouse E-Cadherin Antibody (IF, 1μg/ml)	R&D	Cat#AF748; RRID: AB_355568
Rabbit Anti-DNMT3L (IF, 1:500)	A gift from Dr. Yamanaka	N/A
Mouse Anti-NANOS2 (IF, 1:200)	Suzuki et al. (2007)	N/A
Rabbit Anti-STRA8 antibody (IF, 1:200)	abcam	Cat#ab49602; RRID: AB_945678
Rabbit Anti-Ki-67 Recombinant Monoclonal Antibody (SP6) (IF, 1:200)	Invitrogen	Cat#MA5-14520; RRID: AB_10979488
Rat Anti-Ki67 Monoclonal Antibody (SolA15) (IF, 1:100)	Invitrogen	Cat#14-5698-82; RRID: AB_10854564
Mouse Anti-phospho-histone H3 (ser10) (IF, 1:200)	Millipore	Cat#06-570; RRID: AB_310177
Rabbit Anti-phospho-S6 Ribosomal Protein (Ser235/236) (IF, 1:200)	Cell Signaling Technology	Cat#2211; RRID: AB_331679
Mouse Anti-ACTB (WB, 1:1000)	Sigma-Aldrich	
Rabbit Anti-DND1 (WB, 1:1000)	A gift from Dr. Suzuki (Suzuki et al., 2016)	N/A
Mouse Anti-FLAG M2 Monoclonal HRP-conjugated (WB, 1:5000)	Sigma-Aldrich	Cat#A8592; RRID: AB_439702
Donkey Anti-Rat IgG Alexa 488 (IF, 1:1000)	Invitrogen	Cat#A-21208; RRID: AB_2535794
Donkey Anti-Rat IgG Alexa 594 (IF, 1:1000)	Invitrogen	Cat#A-21209; RRID AB_2535795
Donkey Anti-Mouse IgG Alexa 594 (IF, 1:1000)	Invitrogen	Cat#A32744; RRID: AB_2762826
Donkey Anti-Goat IgG Alexa 488 (IF, 1:1000)	Invitrogen	Cat#A32814; RRID: AB_2762838
Donkey Anti-Rabbit IgG Alexa 594 (IF, 1:1000)	Invitrogen	Cat#A-21207; RRID: AB_141637
Donkey Anti-Mouse IgG Alexa 588 (IF, 1:1000)	Invitrogen	Cat#A32766; RRID: AB_2762823
Donkey Anti-Rabbit IgG Alexa 647 (IF, 1:1000)	Invitrogen	Cat#A32795; RRID: AB_2762835
Donkey Anti-Rabbit IgG Alexa 594 (IF, 1:1000)	Invitrogen	Cat#32754; RRID: AB_2762827
Donkey Anti-Mouse IgG Alexa 647 (IF, 1:1000)	Invitrogen	Cat#A32787; RRID: AB_2762830
Donkey Anti-Rat IgG Alexa 488 (IF, 1:1000)	Invitrogen	Cat#A32790; RRID: AB_2762833
Goat Anti-Rabbit IgG HRP-conjugated (WB, 1:3000)	Cell Signaling Technology	Cat#7074; RRID: AB_2099233
Horse Anti-mouse IgG HRP-conjugated (WB, 1:3000)	Cell Signaling Technology	Cat#7076; RRID: AB_330924
Bacterial and Virus Strains		
E.coli Strain DH10B	NEB	Cat#C3019
Chemicals, Peptides, and Recombinant Proteins		
M2 medium	Sigma-Aldrich	Cat#M7176
Trypsin-EDTA (0.5%), no phenol red	Gibco	Cat#15400054
DMEM	Gibco	Cat#12430054
Penicillin-Streptomycin (5000U/ml)	Gibco	Cat#15140122

(*Continued on next page*)

Continued

REAGENT or RESOURCE	SOURCE	IDENTIFIER
FBS	HyClone/Cytiva	Cat#SH30070.03
Triton X-100	Sigma-Aldrich	Cat#T9284
Tissue-Tek O.C.T. Compound	Sakura Finetek	Cat#4583
Target Retrieval Solution (10x)	Dako	Cat#S1699
Tween 20	Sigma-Aldrich	Cat#P9416
CellStain DAPI (4′, 6′-Diamidino-2-phenilindole Dihydrochloride)	FUJI FILM	Cat#342-07431
Bovine Serum Albumin	Sigma-Aldrich	Cat#A7030
Lipofectamine2000	Thermo Fisher Scientific	Cat#11668019
Opti-MEM | Reduced Serum Media	Thermo Fisher Scientific	Cat#319085070
Doxycyclin hyclate	Sigma-Aldrich	Cat#D9891
Recombinant RNase inhibitor	Takara Bio	Cat#2313
cOmplete Mini, EDTA-free Protease Inhibitor	Roche	Cat#4693159001
Nonidet P40	Nakarai	Cat#23640-94
Anti-FLAG-M2 affinity gel	Sigma-Aldrich	Cat#A2220
RNAiso Plus	Takara Bio	Cat#9190
Critical Commercial Assays		
NEBuilder HiFi DNA Assembly Master Mix	NEB	Cat#E2621
Chromium Single Cell 3′ Reagent Kit v2	10x Genomics	Cat#PN-120237
RNeasy Mini Kit	QIAGEN	Cat#74104
Super script IV	Thermo Fisher Scientific	Cat#18090050
KAPA SYBR Fast qPCR kit	KAPA Biosystems	Cat#KK4618
Deposited Data		
Raw sequence data of scRNA-seq data	This paper	DNA Data Bank of Japan: DRA011172
RNA-seq of *Nanos2*-KO male germ cells and *Ddx6*-cKO	Shimada et al. (2019)	DNA Data Bank of Japan: DRA007505
Data set of scRNA-seq for NIH-3T3	10x Genomics	https://www.10xgenomics.com/resources/datasets?query=&page=1&configure%5Bfacets%5D%5B0%5D=chemistryVersionAndThroughput&configure%5Bfacets%5D%5B1%5D=pipeline.version&configure%5BhitsPerPage%5D=500
Experimental Models: Cell Lines		
NIH/3T3	ATCC	CRL-1658
ciN2D1-3T3	Hirano et al., in revision	N/A
Experimental Models: Organisms/Strains		
Mouse: MCH	CLEA Japan	N/A
Mouse: *floxed-Dazl:* $Dazl^{tm2a(KOMP)Wtsi}$	Fukuda et al. (2018)	N/A
Mouse: *Oct4dPE-CreER*^{T2}	A gift from Dr. Suzuki	N/A
Mouse: *Nanos2*-KO	Tsuda et al. (2003)	N/A
Mouse: *Nanos2-mCherry*	Wright et al. (2021)	N/A
Oligonucleotides		
Primers for genotyping and RT-qPCR	See Table S11	N/A
Recombinant DNA		
CS-dual-EmGFP	This study	N/A
CS-dual-EmGFP-*Actb 3′UTR*	This study	N/A
CS-dual-EmGFP-*Dazl 3′UTR*	This study	N/A

(*Continued on next page*)

Continued

REAGENT or RESOURCE	SOURCE	IDENTIFIER
CS-dual-EmGFP-*Rheb 3'UTR*	This study	N/A
CS-dual-EmGFP-*Anp32b 3'UTR*	This study	N/A
CS-dual-EmGFP-*Ptma 3'UTR*	This study	N/A
Software and Algorithms		
ImageJ/Fiji ver. 2.1.0/1.53c	Schindelin et al. (2012)	https://imagej.net/software/fiji/
ApE- A plasmid Editor v2.0.61	M. Wayne Davis	https://jorgensen.biology.utah.edu/wayned/ape/
Cellranger	10x Genomics	https://support.10xgenomics.com/single-cell-gene-expression/software/overview/welcome
R ver. 3.6.2	R Core Team (2019)	https://www.r-project.org/
R studio	RStudio Team (2018)	https://www.rstudio.com/
Python 3.7.3	Van Rossum and Drake (2009)	https://www.python.org/downloads/
Seurat v2.3.4	Butler et al. (2018)	https://satijalab.org/seurat/
monocle v2.14.0	Trapnell et al. (2014), Qiu et al., 2017a, 2017b	http://cole-trapnell-lab.github.io/monocle-release/
Velocyto	La Manno et al. (2018)	http://velocyto.org/

RESOURCE AVAILABILITY

Lead contact

Further information and requests for resources and reagents should be directed to and will be fulfilled by the lead contact, Yumiko Saga (ysaga@nig.ac.jp).

Materials availability

All unique/stable reagents generated in this study are available from the Lead Contact with a completed Materials and Transfer Agreement.

Data availability

Raw data sequence data generated in this study and previous study (Shimada et al., 2019) were publicly available. Accession numbers are listed in the key resources table. The scRNA-seq data for NIH/3T3 cells were available from the homepage of 10x Genomics. URL were listed in the key resources table.

EXPERIMENTAL MODEL AND SUBJECT DETAILS

Animals

All mouse experiments were approved by the National Institute of Genetics (NIG) Institutional Animal Care and Use Committee. Mice were housed in a specific pathogen-free animal care facility at NIG. To recover embryonic samples, we crossed reproductively active female (8-20 weeks-old) with over 8 weeks-old male mice. For the analysis of *Nanos2*-KO, *Nanos2* KO (Tsuda et al., 2003) or *Nanos2*-mCherry (Wright et al., 2021) mice lines were used. The embryos were collected from pregnant female at E13.5, E14.5 and E15.5. To generate *Dazl*-cKO embryo, floxed-*Dazl* (Fukuda et al., 2018) homozygous female were crossed with floxed-*Dazl*; *Oct4dPE*-Cre-ER^{T2} (provided by A. Suzuki, Yokohama National University) male mice and 500 μl of 10 mg/ml tamoxifen (Sigma-Aldrich, T5648) was intraperitoneally injected to pregnant female at E12.5 and collected sample at E15.5. For scRNA-seq analysis, MCH (provided by CLEA Japan, Inc.) females were crossed with male and embryos were collected at E11.5, E12.5, E13.5, E14.5 and E15.5. Whenever possible, each mutant mouse was compared to control littermates or age-matched non-littermates from the same colony. All mice were handled and propagated in accordance with the guidelines of the National Institute of Genetics (NIG), and all experimental procedures were approved by the Committee for Animal Care and Use of NIG.

Cell lines

In this study, we used the Dox-inducible NANOS2-DND1 NIH-3T3 cell line (ciN2D1-3T3), which was established in our laboratory using the piggyBac transposon system (Hirano et al., manuscript in preparation). ciN2D1-3T3 were cultured in high-glucose DMEM (Thermo) containing 10% FBS and Pen Strep (Gibco).

METHOD DETAILS

Preparation of germ cell spreads

Germ cell spreads were prepared from E13.5 to E15.5 testes and E15.5 ovaries. Gonads were collected in 700 μl of M2 medium, passed through an 18-G needle and washed with PBS. The samples were incubated with 1 mg/ml of collagenase Type I (Invitrogen) at 37°C for 15-30 min, washed with PBS and incubated with 0.15% Trypsin-EDTA for 1 min at 37°C. After washing with 500 μl of DMEM containing 10% (v/v) FCS and with PBS, hypotonic buffer (30 mM Tris-HCl (pH 7.5), 50 mM sucrose, 17 mM trisodium citrate dehydrate, 5 mM EDTA, 0.5 mM DTT and 0.5 mM PMSF) was added and incubated for 30 min at room temperature (RT). After spinning for 3 min at 400 × g, cells were resuspended in 100 mM sucrose containing 1 mM sodium hydroxide. The cell suspension was spread on slide glasses with 1% PFA containing 0.5% Triton X-100. Slide glasses were placed in a humidified slide chamber and incubated at 37°C overnight and then subjected to the immunostaining procedure. The spread germ cells were reacted with primary antibodies overnight at 4°C at the following dilutions: 1:4,000 for rat anti-GCNA (a gift from Dr. Nishimune) (Tanaka et al., 1998), 1:100 for rabbit anti-REC8 (a gift from Dr. Ishiguro, Kumamoto University) (Ishiguro et al., 2011) and 1:200 for mouse anti-phospho-histone H3 (ser10) (a gift from Dr. Kimura, Osaka University) (Hayashi-Takanaka et al., 2009). Secondary antibodies labeled with Alexa Fluor 488, 594 or 647 (1:1,000, Thermo A21209, A32790 and A32787) were used. DNA was counter-stained with DAPI (100 ng/ml). Fluorescence microscopy was performed using Olympus FV1200.

Gonad sample preparation and immunostaining

Embryonic gonads were fixed in 4% PFA for 30 min at 4°C. Gonads were next submerged in 10 and 20% sucrose in PBS for 1 h each at 4°C, and in 30% sucrose in PBS overnight at 4°C. The gonads were then embedded in Tissue-Tek O.C.T. compound (Sakura Finetek) and frozen in liquid nitrogen. Six-micrometer-thick sections of each gonad were applied to glass slides and autoclaved in TRS (Dako). After pre-incubation with 3% skim milk in PBS-T (PBS with 0.1% Tween20 (Sigma-Aldrich)) at RT for 30 min, the sections were reacted with primary antibodies overnight at 4°C at the following dilutions: 1:200 for mouse anti-phospho-histone H3 (ser10) (1:200, Sigma-Aldrich, 06-570), goat anti-CDH1 (1μg/ml, R&D, AF748), rabbit anti-DNMT3L (1:500, provided by Dr. Yamanaka), rabbit anti-STRA8 (1:200, abcam #ab49602), rabbit anti-Ki67 (1:200, Invitrogen #MA5-14520), rat anti-Ki67 (1:100, Invitrogen AB_10854564) and anti-pS6 (1:200, CST #2211). Secondary antibodies labeled with Alexa 488, 594 or 647 (1:1,000, Invitrogen A21207, A21208, A21209, A32766, A32814, A32754, A32744 and A32795) were used. DNA was counter-stained with DAPI (100 ng/ml). Fluorescence microscopy was performed using Olympus FV1200 and images were processed with ImageJ/Fiji (Schindelin et al., 2012).

Flow cytometry

Single-cell suspensions were prepared from testes from E13.5 and E14.5 embryos by incubation with 0.15% trypsin-EDTA at 37°C for 5 min, and then washed with DMEM containing 0.5% BSA (wash medium). After discarding the supernatant, cells were fixed in 100 μl of 4% PFA for 10 min at RT, followed by the addition of 900 μl of cold 100% EtOH and incubated at 4°C overnight. After spinning down for 5 min at 400 × g, cells were washed with wash medium and reacted with primary antibodies for 1 h at RT at the following dilutions: mouse anti-NANOS2 (1:200, (Suzuki et al., 2007)), rabbit anti-Ki67 (1:200, Invitrogen #MA5-14520) and rat anti-GCNA (1:4,000, a gift from Y. Nishimune, Osaka University). Then, cells were washed with wash medium and reacted with secondary antibodies labeled with Alexa Fluor 488, 594 or 647 (1:1,000, Invitrogen A32766, A21209 and A32795) for 30 min at RT. Next, washed cells were re-suspended in 0.1% BSA-containing PBS and analyzed by a JSAN Desktop Cell Sorter or SH800 (SONY). The data were visualized using flowCore package (Ellis et al., 2019).

Single-cell RNA-seq

Single-cell suspensions were prepared from 6-26 gonads from E11.5-E15.5 embryos by incubation with 0.15% trypsin-EDTA at 37°C for 5-10 min. The E11.5 embryos were genotyped to determine the sex using primers to detect *Ube1*, as described in a previous report (Chuma and Nakatsuji 2001). After incubation,

wash medium was added to inhibit trypsin and cells were filtered through a 35-μm sieve (BD Bioscience). Cells were re-suspended in DMEM containing 10% FBS and the cell density was adjusted to 1.0×10^6 cells/ml. We aimed to load 3,000 cells on the Chromium™ Controller (10x Genomics Inc.) and constructed the scRNA-seq libraries using Chromium™ Single Cell 3' Reagent Kits v2 following the manufacturer's instructions. Each library was read at a depth of 1 million per sample for cell number estimation and 100 million per sample for analysis using Hiseq2500. After cell number estimation, we found that the library derived from E14.5 ovarian cells contained over 10,000 cells. This may have been due to a technical issue. As an excessive cell number reduces the sequence depth per cell, we did not conduct deep sequencing for the E14.5 female sample.

RNA immunoprecipitation and reverse-transcription quantitative PCR

For RNA immunoprecipitation followed by reverse-transcription quantitative PCR (RT-qPCR) analysis, NANOS2-DND1 expression was induced by Dox (0.5 μg/ml) addition into ciN2D1-3T3 in ϕ10-cm dishes. After collecting cells by trypsin (0.15 mg/ml) treatment for 3 min at 37°C, cells were washed with PBS and lysed in 1 ml of Buffer A (50 mM Tris-HCL (pH 7.4), 150 mM NaCl, 0.5% NP40, 7.5 mM β-glycerophosphate, 1 mM EDTA, 1 mM DTT and 400 units/ml of Recombinant RNase Inhibitor (TaKaRa)) with cOmplete (Roche) on ice for 10 min and spun at 150,000 rpm for 10 min at 4°C. Twenty microliters of anti-FLAG M2 affinity gel (Sigma) was added to the supernatant and incubated for 3 h at 4°C. After 5 washes with Buffer A, co-precipitated RNAs were purified using the RNeasy Mini Kit (Qiagen). After the synthesis of first-strand cDNAs with 200 U of Superscript IV reverse transcriptase (Invitrogen) and 0.25 μg of oligo dT primer, RT-qPCR analyses were carried out with KAPA SYBR FAST qPCR kits using a Thermal Cycler Dice Real Time System (TaKaRa) according to the manufacturer's instructions. The expression level of mRNA of interest was normalized by *Gapdh*. Then, the fold enrichment of each mRNA in the IP compared with the input was calculated. We repeated 5 independent experiments and analyzed the data using Dunnett's comparison by employing the glht function from the multcomp package (Hothorn et al., 2008). The immunoprecipitated proteins were run on 12% acrylamide gel and Western blotting was performed using mouse anti-ACTB (1:1,000, Sigma) followed by HRP-conjugated secondary antibody or HRP-conjugated anti-FLAG M2 (1:5,000, Sigma A8592). After ACTB detection, the membrane was directly used to detect DND1 with rabbit anti-DND1 (a gift from A. Suzuki, Yokohama National University), followed by the HRP-conjugated secondary antibody.

Functional assessment of 3'UTR using the dual reporter system

The 3'UTR of each gene was cloned downstream of the *Emgfp* sequence in the dual reporter vector and the transgenes were introduced into ciN2D1-3T3 cells. One day after transfection of 1 μg of the vector using Lipofectamine 2000 (Invitrogen), cells were treated with Dox (0.5 μg/ml) or DMSO for 1 day. Then, cells were collected using RNAiso Plus (TaKaRa) and RNAs were purified. After the synthesis of first-strand cDNAs with 200 U of Superscpript IV reverse transcriptase (Invitrogen) and 0.5 μg of oligo dT primer, RT-qPCR analyses were performed according to manufacturer's instructions. The expression level of *Emgfp* was normalized by that of *mCherry* and the fold change of each 3'UTR to *Actb* 3'UTR was calculated. We repeated 3 independent experiments and analyzed the data using Dunnett's comparison by employing the glht function from the multcomp package (Hothorn et al., 2008).

QUANTIFICATION AND STATISTICAL ANALYSIS

Statistical analysis was performed using R.

Figure 1B: The proportion of Ki67-positive germ cells (Control: n=18, *Nanos2* $^{-/-}$: n=12 and dKO n=6). Bar graph indicates mean with SD. P-value (Dunnett's test) less than 0.05 were considered as statistically significant difference. Asterisks indicate p-value less than 0.001 (***) and 0.05 (*).

Figures 3C and 3F: The gene expression of each population was shown as violin plot and median was shown as dot.

Figure 5E: The expression changes in *Nanos2* $^{-/-}$ and *Ddx6* $^{-/-}$ male germ cells. Bar graph indicates log2 fold change. P-value (Wald test) less than 0.05 were considered as statistically significant difference. Asterisks indicate p-value less than 0.001 (***), 0.01 (**) and 0.05 (*).

Figure 5F: The expression of each population was shown as violin plot and median was shown as dot. P-value (Wilcoxon rank-sum test) less than 0.05 were considered as statistically significant difference. *** indicates p-value less than 0.001. The p-value for each spliced and unspliced transcript are as follows; *Rheb* 5.83e-25 (E13.5, spliced), 0.958 (E13.5, unspliced) and 5.01e-28 (E14.5, spliced) and 0.0842 (E14.5, unspliced); *Anp32b* 1.51e-12 (E13.5, spliced), 0.939 (E13.5, unspliced) and 3.97e-29 (E14.5, spliced), 0.309 (E14.5, unspliced) and *Ptma* 2.96-30 (E13.5, spliced), 0.0630 (E13.5, unspliced), 3.97e-29 (E14.5, spliced) and 0.110 (E14.5, unspliced).

Figure 6B: The proportion of pS6 single positive and pS6 and Ki67 double-positive germ cells (*Nanos2* $^{+/-}$: n=4 and *Nanos2* $^{-/-}$: n=4). Bar graph indicates mean with SD. P-value (t test) less than 0.05 were considered as statistically significant difference. * indicates p-value less than 0.05.

Figure 6C: The Fold enrichment of target genes in IP sample (*Actb*: n=5, *Rheb*: n=5, *Anp32b*: n=5 and *Ptma*: n=5). Bar graph indicates mean with SD. P-value (Dunnett's test) less than 0.05 were considered as statistically significant difference with *Actb*. Asterisks indicate p-value less than 0.01 (**) and 0.05 (*).

Figure 6D: The relative expression of GFP to mCherry (3'UTR of *Actb*: n=3, *Dazl*: n=3, *Rheb*: n=3, *Anp32b*: n=3 and *Ptma*: n=3). Bar graph indicates mean with SD. P-value (Dunnett's test) less than 0.05 were considered as statistically significant difference with 3'UTR of *Actb*. Asterisks indicate p-value less than 0.01(**) and 0.05 (*).

Figure S11C: The expression of each population was shown as violin plot and median was shown as dot. P-value (Wilcoxon rank-sum test) less than 0.05 were considered as statistically significant difference. *** indicates p-value less than 0.001.

Figure S14B: The gene expression in NIH-3T3 was shown as violin plot and median was shown as dot.

Figure S15C: The relative expression of GFP to mCherry (3'UTR of *Actb*: n=3, *Dazl*: n=3, *Rheb*: n=3, *Anp32b*: n=3 and *Ptma*: n=3). Bar graph indicates mean with SD. P-value (Dunnett's test) less than 0.05 were considered as statistically significant difference with 3'UTR of *Actb*. * indicate p-value less than 0.05.

Statistical analysis of scRNA-seq

Fastq files were processed and aligned to the mouse mm10 transcriptome using the 10X Genomics Cell Ranger v2.1.1 pipeline. Further analyses were conducted on R (ver. 3.6.2) and RStudio (ver.1.2.1335) (R Core Team, 2019; RStudio Team 2018). Quality assessment of scRNA-seq data and analyses were conducted using the Seurat package for R following the developer's tutorial (Butler et al., 2018). Briefly, all data were merged into a single data set and log normalization was performed. The cells in which the detected gene number was less than 10% among all cells and those that contained more than 5% mitochondrial genes were eliminated. Then, only cells that expressed more than 200 genes were used for further analysis to remove the effects of low-quality cells. For clustering analysis, significant principal components were estimated using JackStrawPlot and PCElbowPlot functions built in Seurat, and those with a $P < 0.01$ were selected from PC1-20 and used for clustering. Using the FindMarkers function in Seurat, differentially expressed genes were identified using the threshold of an adjusted P-value of 0.1 and log fold change of 0 in addition to default settings. Pseudo-time analyses were conducted using the monocle package for R following the developer's tutorial (Trapnell et al., 2014; Qiu et al. 2017a, 2017b). RNA velocity analysis was conducted using the RNA velocyto package for python (Python 3.7.3 (Van Rossum and Drake 2009)) and R (La Manno et al., 2018) with default settings, and visualized on tSNE plots built in Seurat.

Cell cycle analysis of germ cells

Cell cycle estimation using scRNA-seq data was conducted using the method previously reported by Macosko et al. and Kashima et al. (Macosko et al., 2015; Kashima et al., 2018). Five cell cycle phases (G1/S, S, G2, G2/M and M/G1) reflecting gene sets were obtained from Whitfield et al. (Whitfield et al., 2002). Genes assigned to the GO term, "meiosis I cell cycle process" were also obtained. From these obtained genes, we excluded those with a low correlation with all genes in the same group in the wild-type germ cells (R<0.2). The selected genes are listed in Table S10. The average expression of the selected genes in each cell was calculated to define the score for each phase. These scores were scaled to obtain a pattern of phase-specific scores for all germ cells. Then, we compared the pattern of phase-specific scores with 13 potential

patterns. We generated 6 simple potential patterns (G1/S, S, G2, G2/M, M/G1 and meiosis), all positive, all negative and 5 intermediate patterns (G1/S-S, S-G2, G2-G2/M, G2/M-M/G1 and M/G1-G1/S) using the 75th and 25th percentiles of scores as positive and negative signals, respectively. Each cell was assigned a phase with the highest correlation score. Cells assigned to G1/S and G1/S-S were finally assigned to G1/S, those in S to S, those in S/G2 to S/G2, those in G2 to G2, those in G2-G2/M, G2/M, G2/M-M/G1, M/G1 to G2/M/G1, those in M/G1-G1/S to G1, those in meiosis to meiosis, and those in all positive and all negative to unclassified (G0). In Figure S16, each cell cycle score is shown as a heat plot (A) and tSNE-plot (B) using genes listed in Table S10.

Identification of post-transcriptionally regulated gene candidates

To identify post-transcriptionally regulated genes, gene expression changes in *Nanos2*$^{-/-}$ cells at E13.5 and E14.5 compared with control were examined for both spliced and unspliced transcripts. For this purpose, we merged unspliced transcript-derived UMI counts contained in the output file of velocyto with the raw count matrix of a Seurat object, and then normalized it using the NormalizeData function in Seurat. Using the FindMarkers function in Seurat, expression changes for both spliced (Table S3 for E13.5 and S4 for E14.5) and unspliced transcripts (Table S7 for E13.5 and S8 for E14.5) were calculated. To identified post-transcriptionally regulated genes, we only focused on genes detected in both spliced and unspliced form. Therefore, our analysis does not contain genes which lack the unspliced form (e.g. single exon genes and weakly expressed genes). The genes identified as differentially expressed among spliced but not unspliced transcripts were obtained as primary candidates of post-transcriptionally regulated genes. Genes regulated by NANOS2 are expected to exhibit consistent changes at both E13.5 and E14.5 in *Nanos2*$^{-/-}$. Therefore, we further focused on genes up-regulated at both time points as suppressed candidates and those down-regulated at both time points as activated candidates.

Gene enrichment analysis

To characterize the major gene expression changes in mutant cells, we utilized Metascape (Zhou et al., 2019) with default settings and visualized the results using the GOplot package for R (Walter et al., 2015).

RNA-seq re-analysis

The previously reported RNA-seq data were prepared as previously described (Shimada et al., 2019). Gene expression changes were calculated using DESeq2 (Love et al., 2014) and visualized using the ggplot package for R.